

Model Based Imaging

Charles A. Bouman

School of Electrical and Computer Engineering
Purdue University

Laurence Livermore National Laboratory
2013-05-21

Co-authored with:

Ken Sauer, University of Notre Dame

Jean-Baptiste Thibault, GE Healthcare

Jiang Hsieh, GE Healthcare

Zhou Yu, GE Healthcare

Venkat Venkatakrisnan, Purdue

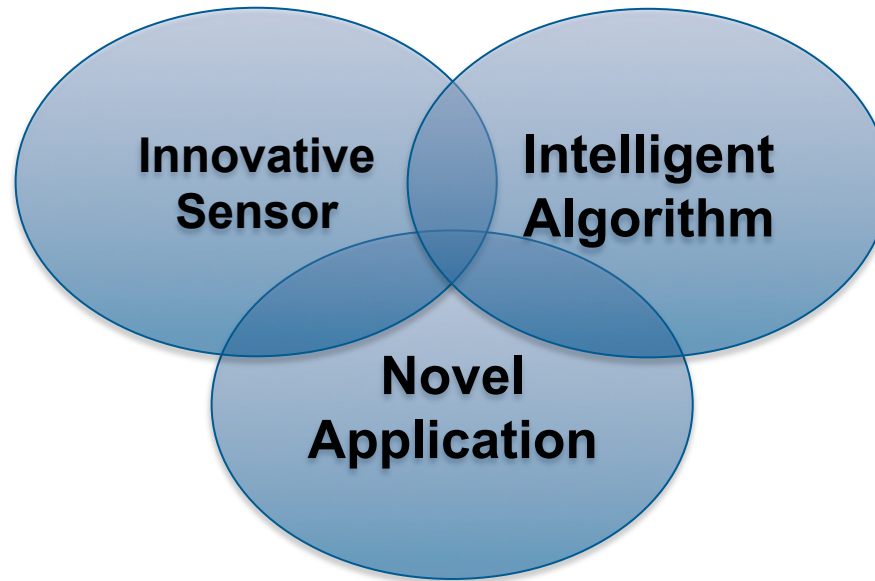
Larry Drummy, AFRL

Marc De Graef, CMU

Jeff Simmons, AFRL

Brendt Wohlberg, LANL

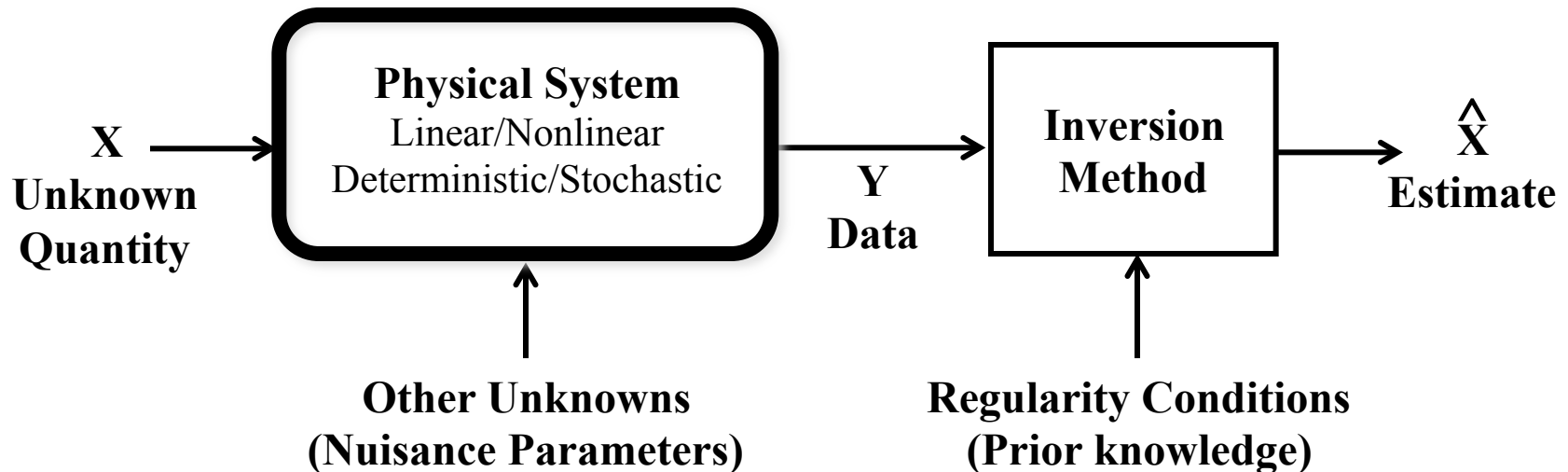
Integrated Imaging: Combining Algorithms and Physical Sensors



- Traditional sensor design is reaching its limits
 - Difficult to only measure one parameter
 - No longer possible to “fix” the device
- Rather than making the “purest” measurement, make the most informative measurement.
- Emerging examples: Computational photography; multiview imaging; tomography; hyperspectral imaging; 4D imaging;

Inverse Problems in Imaging

- Recover information from indirect measurements
 - Image deblurring
 - Tomography
 - 3D scene recovery and human vision



- *Image and system models are critical to accurate inversion*

Inverse Problem: Example



■ Forward model

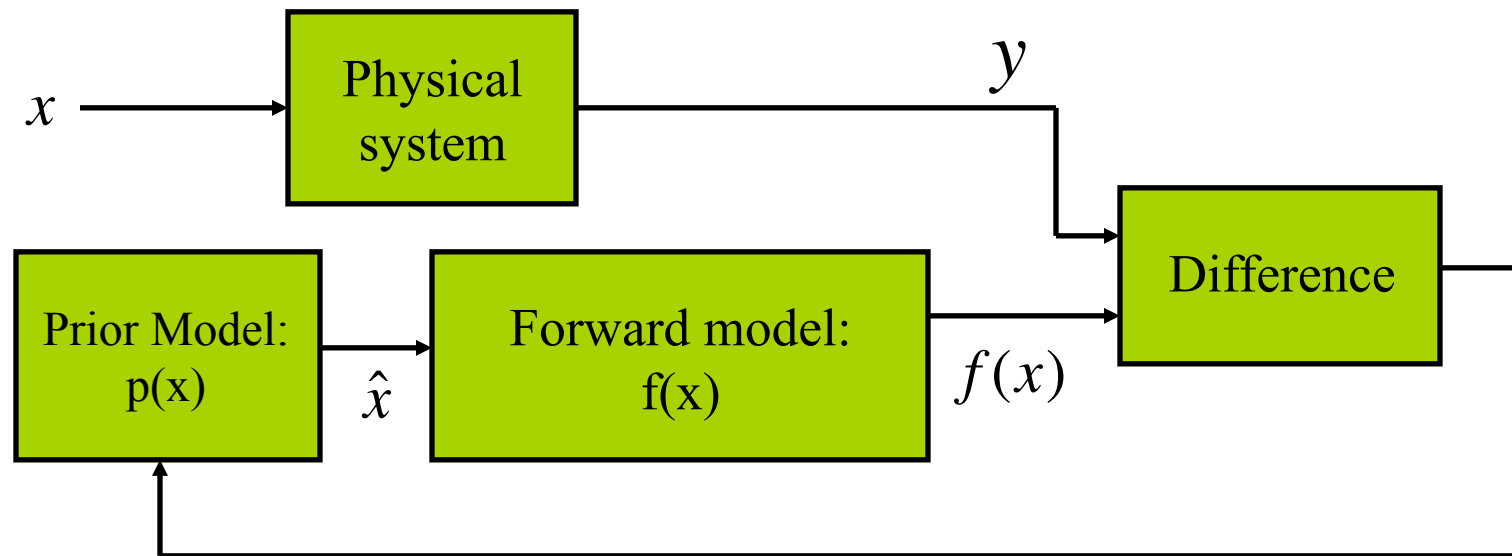
- Gravity
- Fluid dynamics
- Light propagation
- Image formation

■ Inversion

- Illumination estimation
- Shape from X
- Inverse dynamics
- Real world knowledge

- Inverse Solution: Something fell in the water

Model Based Iterative Reconstruction (MBIR): A General Framework for Solving Inverse Problems



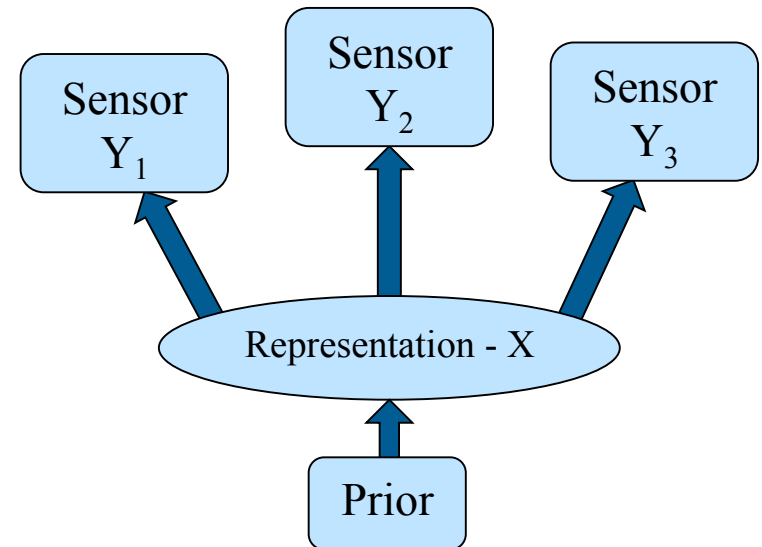
$$\hat{x} \leftarrow \arg \max_x \left\{ \log p(y | x) + \log p(x) \right\}$$

x forward model prior model

\hat{x} – Reconstructed object

y – Measurements from physical system

Model-Based Data Fusion: Estimation



- MAP with parameter estimation

$$\hat{x} = \arg \min_{x \in \Omega} \min_{\phi} \left(-\log p(x) - \sum_{k=1}^K \log p(y_k | x, \phi_k) \right)$$

(not always a consistent estimator,)

- What sensors or combination of sensors have the most information for the problem of interest?

What opportunities does MBIR offer?

- A general framework for sensing
 - Image formation from both linear and nonlinear measurements
 - Data fusion
 - Dynamic sampling
- Allows for the precise modeling of sensor
 - Geometry and transfer function
 - Noise modeling
 - Linear and nonlinear systems
- Explicitly incorporates prior model
 - Can dramatically reduce variance
 - Can incorporate physical models of target
- Adapts to unknowns
 - Automatic calibration of instrument
 - Adaptive modeling of sample

Model-Based Imaging: Modeling Philosophy

“Purity”

Maximum Likelihood
“No Prior Model”

The law of large
numbers

...Infinite variance

Often not effective

Physics-Based
Models

Acceptable
Modeling Error

But usually not
enough...

“The realm of the unholy”

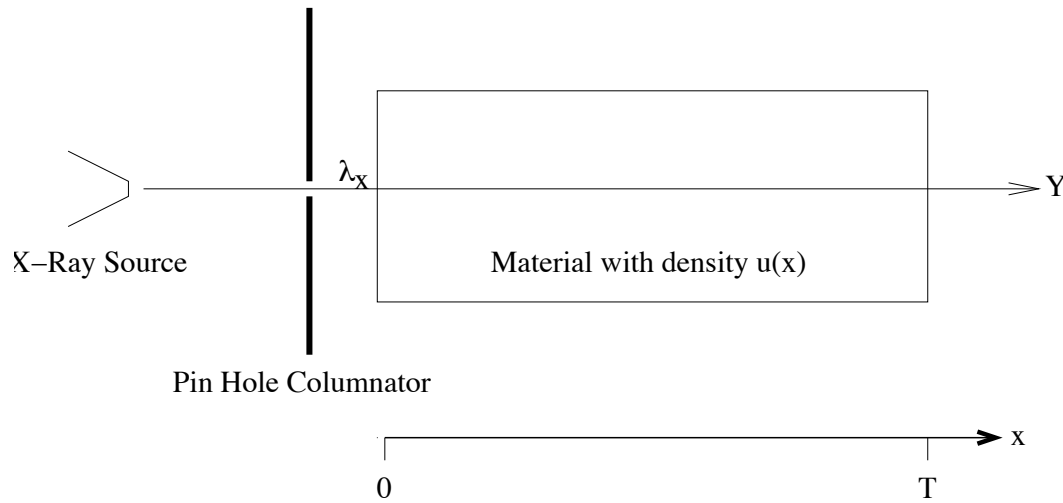
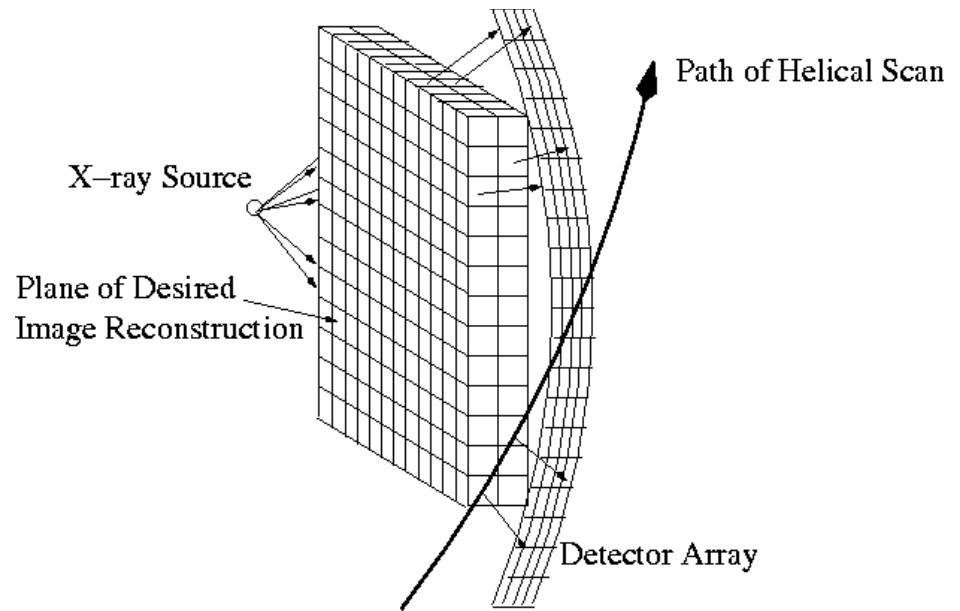
Bizarrely simplistic
priors and ad-hoc
models of information

Heuristic (but clear)
assumptions

Unknown bias

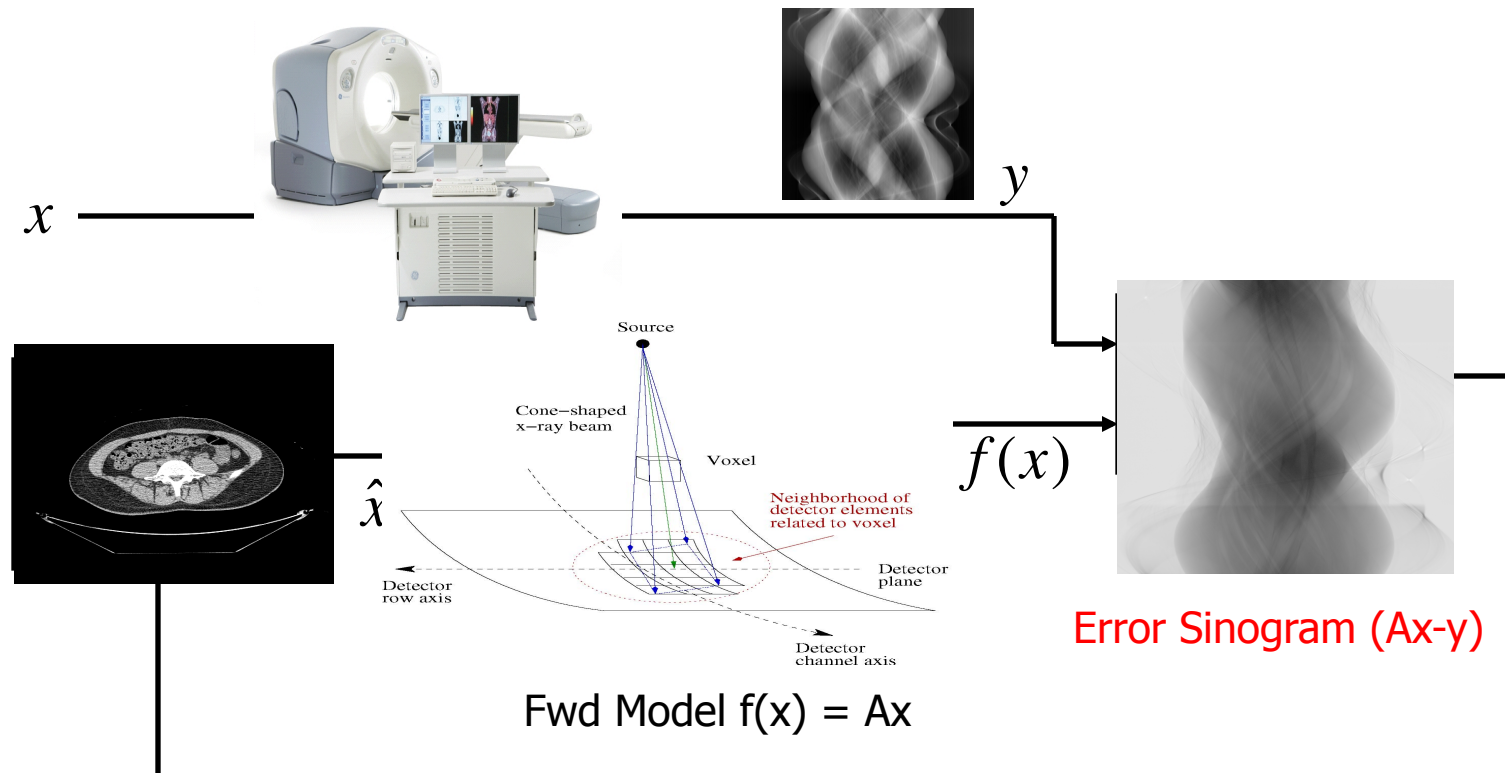
Un-holy, but often
effective...

Multislice Helical Scan CT



$$\int_0^x \mu(t) dt = -\log\left(\frac{\lambda_x}{\lambda_0}\right) + noise$$

Model-Based Iterative Reconstruction (MBIR)

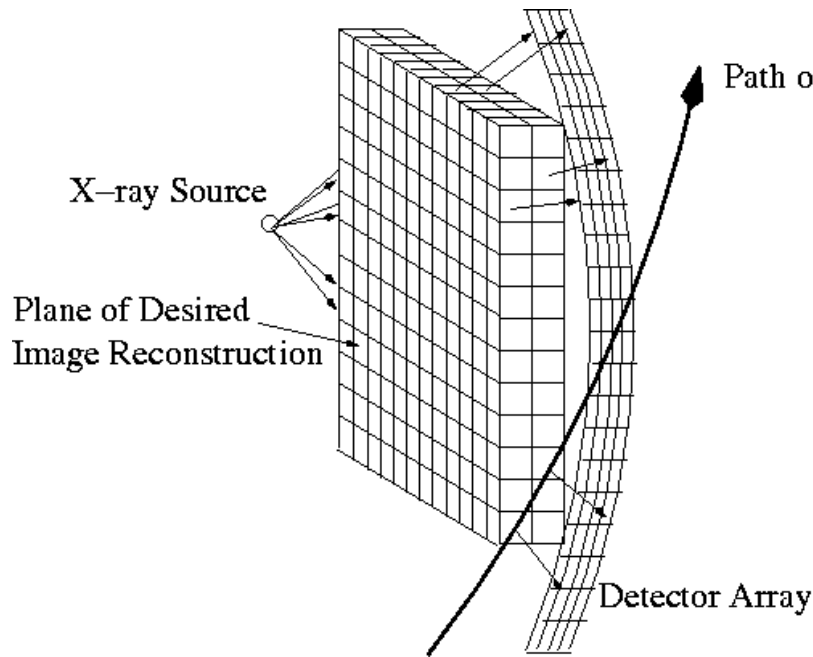


Cost Function $\hat{x} = \arg \min_{x \geq 0} \left\{ \frac{1}{2} (y - Ax)^T \Lambda (y - Ax) + U(x) \right\}$

Model-Based Iterative Reconstruction (MBIR): GE Healthcare's Veo System

- What is Veo?
 - GE announce new product, “Veo”, based on MBIR reconstruction at RSNA 2010
 - System received FDA 510(k) approval in 2011
 - Currently on sale in US as an upgrade option
 - Partnership between GE Healthcare, Purdue University and the University of Notre Dame
 - Research team:
 - Jean-Baptist Thibault, Jiang Hsieh (GE)
 - Ken Sauer (Notre Dame)
 - Me (Purdue)

Scanner Forward Model: $p(y|x)$



λ_i – Photon count at detector

λ_T – Photon dosage

$y_i = \ln\left(\frac{\lambda_T}{\lambda_i}\right)$ – Attenuation measurement

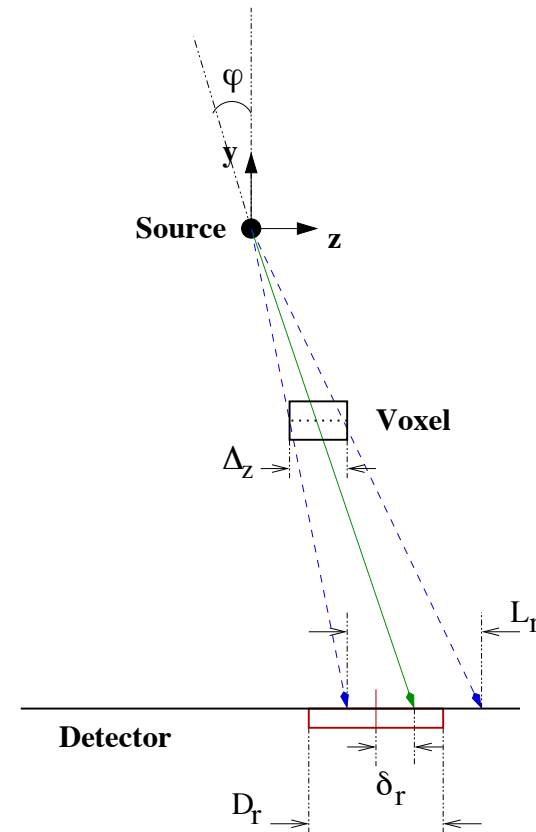
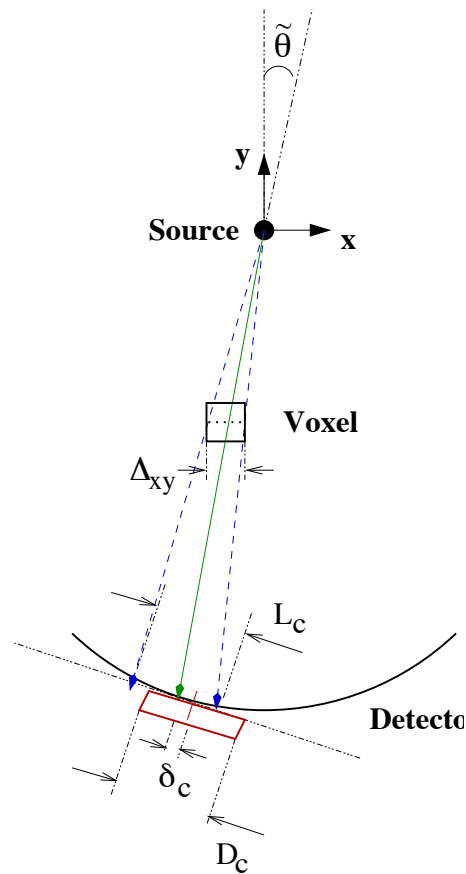
$$E[y_i | x] = \sum_j A_{i,j} x_j \quad - \text{Line integral through object}$$

$$\text{Var}[y_i | x] \cong \frac{\lambda_i + \sigma_e^2}{\lambda_i^2} \quad - \text{Photon counting + electronic noise}$$

Results in: $-\log p(y|x) = \frac{1}{2} \|y - Ax\|_{\Lambda}^2 + \text{constant}$

Distance Driven Projector*

- Fast and accurate projection of 3D voxels

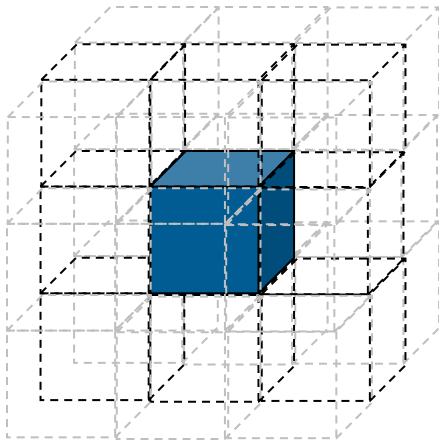


B. DeMan and S. Basu, "Distance-driven projection and backprojection in three-dimensions," *Physics in Medicine and Biology*, vol. 49, pp. 2463–2475, 2004.

Jean-Baptiste Thibault, Ken Sauer, Charles Bouman, and Jiang Hsieh, "A Three-Dimensional Statistical Approach to Improved Image Quality for Multi-Slice Helical CT," *Medical Physics*, pp. 4526-4544, vol. 34, no. 11, November 2007.

Markov Random Field (MRF) Prior Model

- Penalizes difference between neighboring voxels
- 26 point 3D neighborhood used



$$p(x) = \frac{1}{Z} \exp \left\{ - \sum_{\{j,k\} \in C} \rho \left(\frac{x_j - x_k}{\sigma} \right) \right\}$$

$\rho(x_j - x_k)$: Potential function

MRF Potential Functions

$\rho(f_i - f_j)$: Penalty on the difference between neighboring voxels

$$\text{If } \rho(f_i - f_j) = \frac{\left| \frac{f_i - f_j}{\sigma_f} \right|^2}{c + \left| \frac{f_i - f_j}{\sigma_f} \right|^{2-p}}$$

q – Generalized Gaussian MRF*

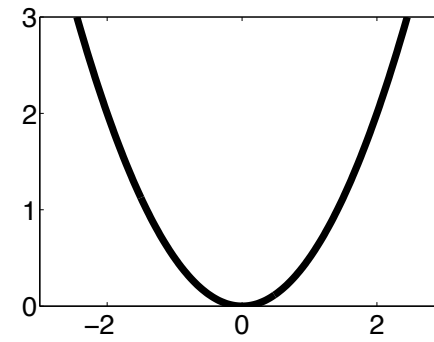
$p = 2$ corresponds to diffuse interfaces

$p = 1$ corresponds to sharp interfaces
- Total Variation Regularization
(compressed sensing)

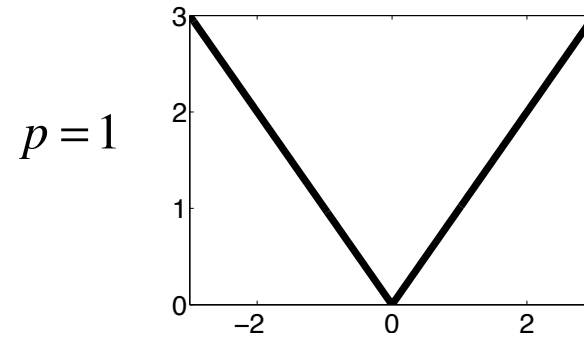
σ_f : MRF scaling parameter (controls noise)

$$\rho(f_i - f_j)$$

Gaussian (L_2) Potential



Total Variation (L_1) Potential



*J.-B. Thibault, K. Sauer, C. Bouman, and J. Hsieh, "A three-dimensional statistical approach to improved image quality for multi-slice helical CT," *Med. Phys.*, vol. 34, no. 11, pp. 4526–4544, 2007

Iterative Coordinate Descent (ICD)

- Iteratively match each pixel (i.e. each column of A)
- Select each pixel to minimize total cost

$$p_i = A_{*,j} x_j$$

$$x_j \leftarrow \arg \min_{x_j} \left\{ \frac{1}{2} \|y - Ax\|_{\Lambda}^2 + U(x) \right\}$$

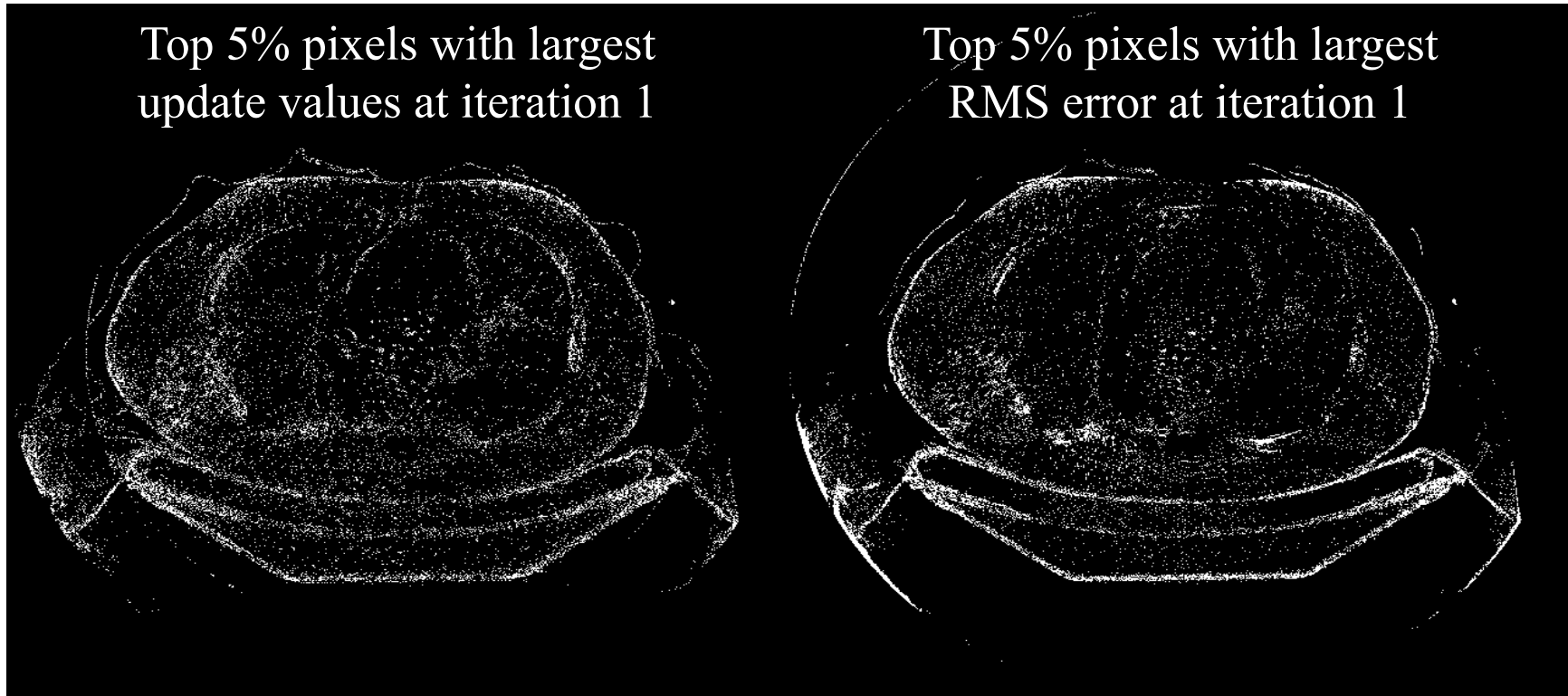
- Issues:
 - Efficient update by using sinogram error state
 - High spatial frequencies converge first
 - Benefits from good initial condition

Why ICD ?

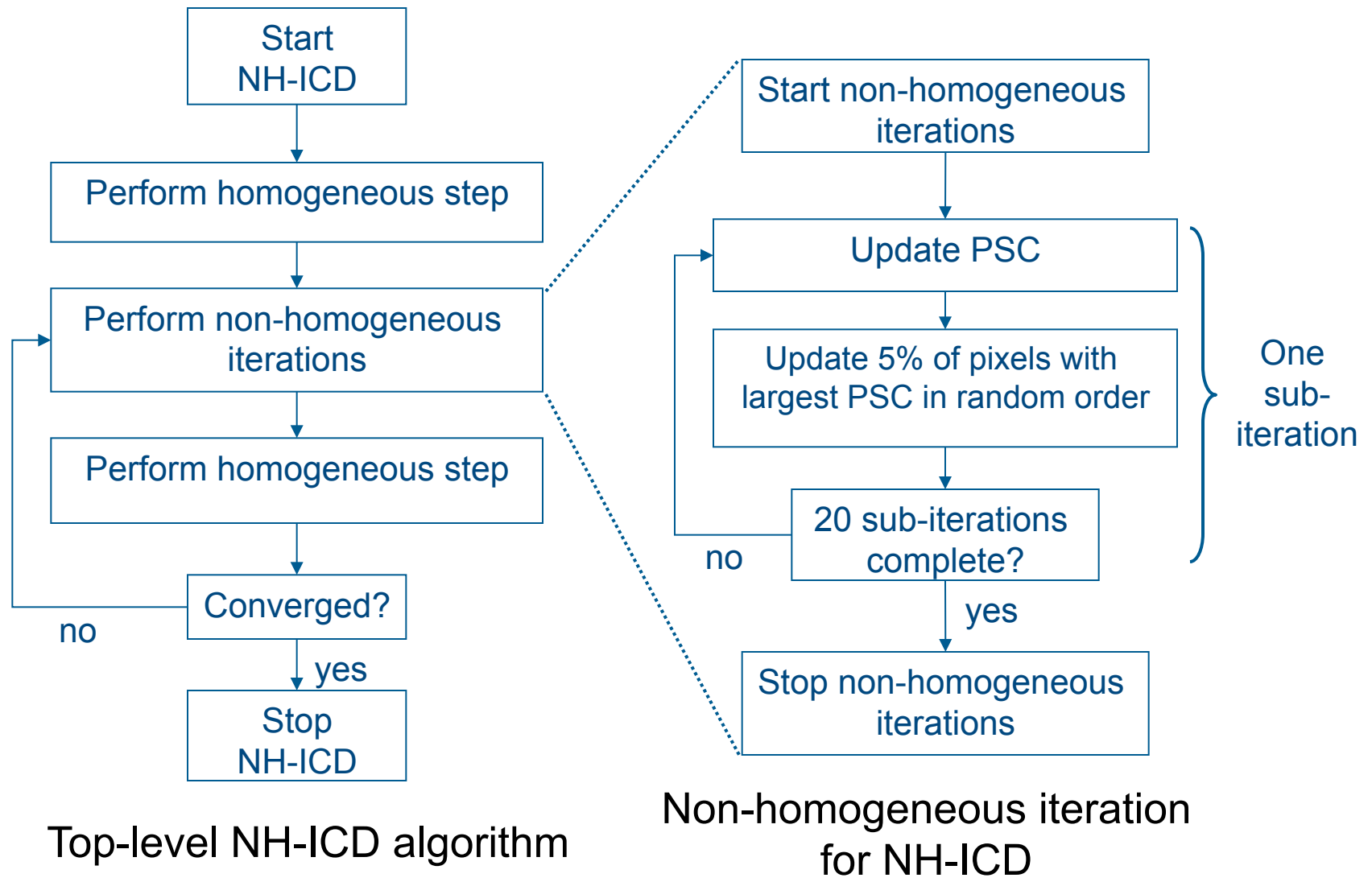
- Advantages:
 - Fast convergence at high spatial frequencies
 - Can be initialized with FBP
 - Sequence of 1D updates provides flexibility
 - Easy to enforce positivity constraints
 - Robust to non-idealities
- Disadvantages
 - Poor low frequency convergence
 - Irregular memory access

Can we make ICD faster using selective updates?

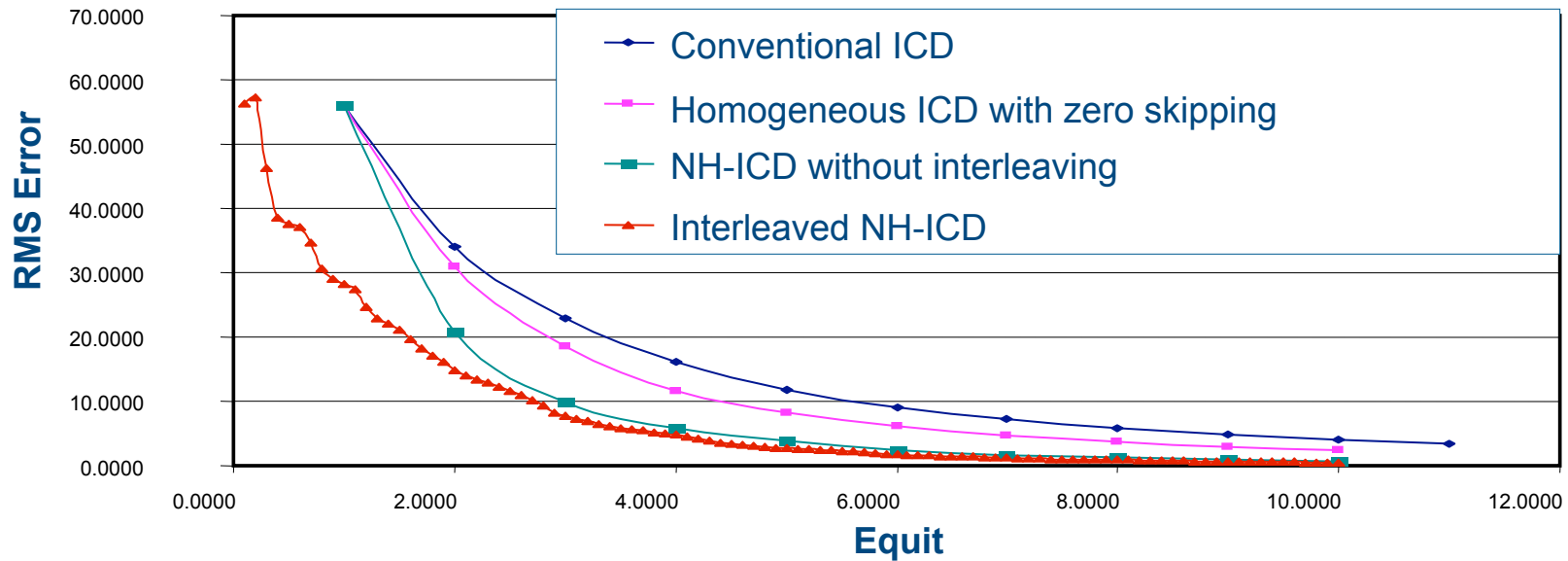
- Objective: find good correlation between update map and true RMS error at different stages of convergence



Non-homogeneous ICD (NH-ICD) Algorithm*



RMSE Convergence Plots for NH-ICD

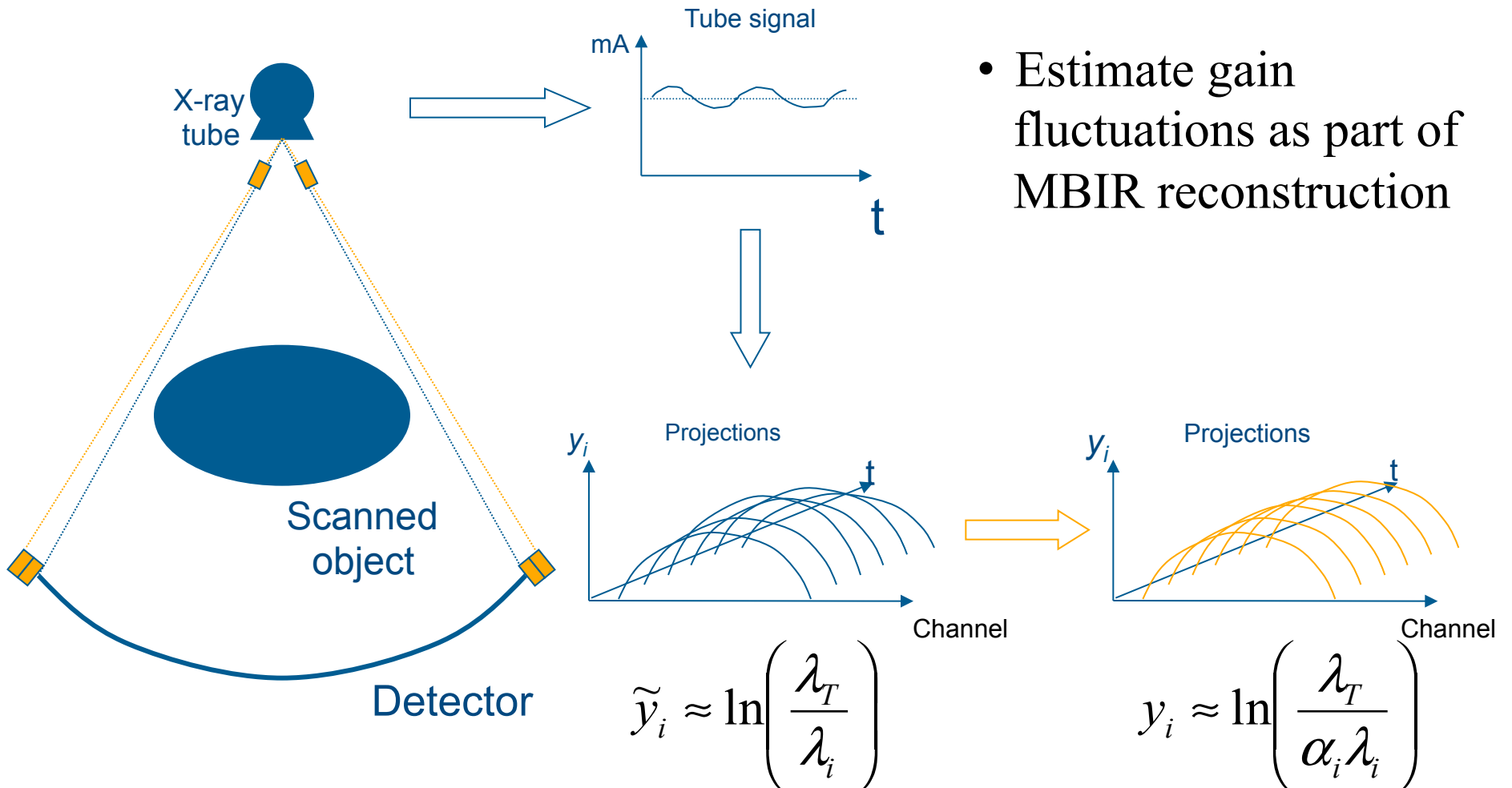


- NH-ICD

- Reduces transients at early stage allowing faster convergence
- Interleaving in early iterations further improves convergence speed

Zhou Yu, Jean-Baptiste Thibault, Charles A. Bouman, Ken D. Sauer, and Jiang Hsieh, "Fast Model-Based X-ray CT Reconstruction Using Spatially Non-Homogeneous ICD Optimization," to appear in the *IEEE Trans. on Image Processing*.

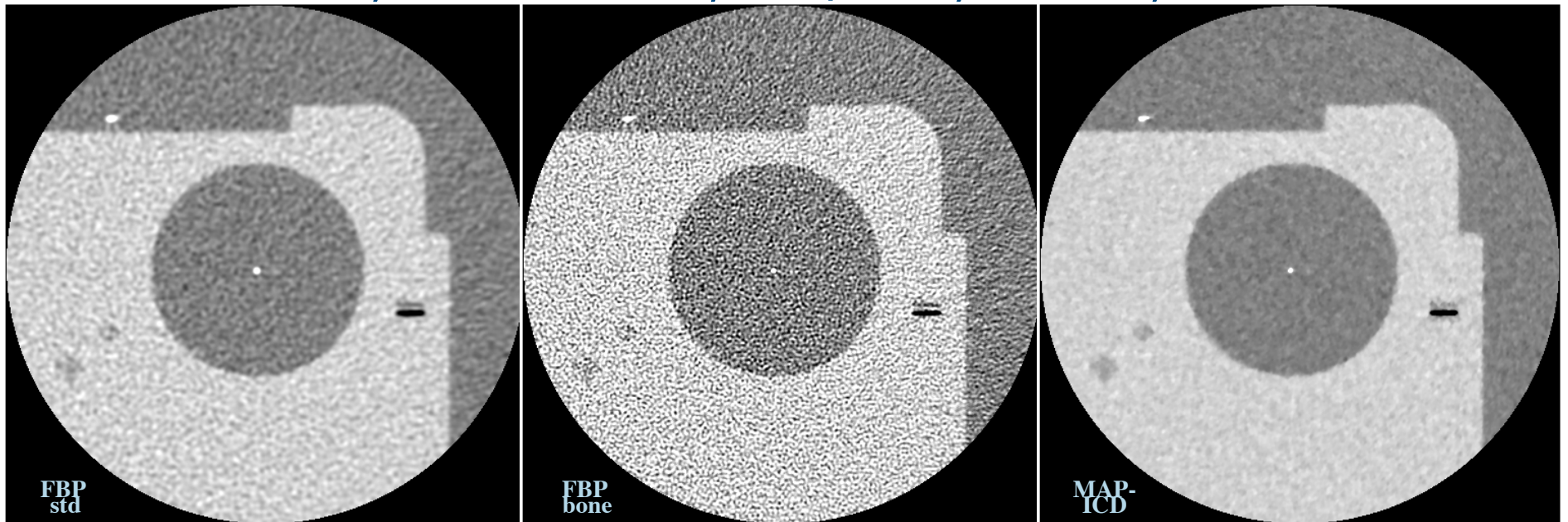
Gain Fluctuations in CT: Example



- Estimate gain fluctuations as part of MBIR reconstruction

Resolution vs Noise

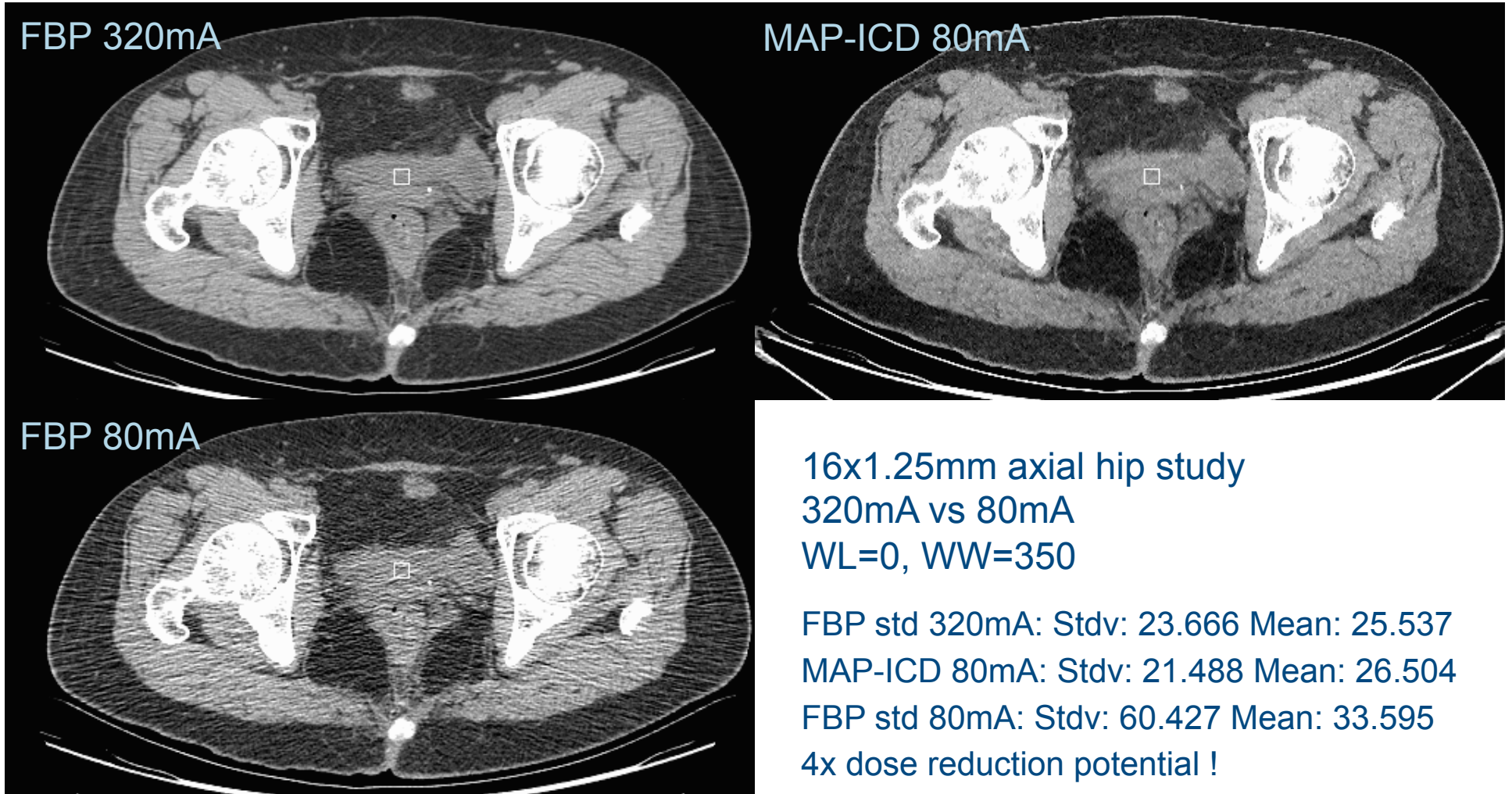
GEPP wire, 16x0.625mm, P15/16:1, 100mA, 10cm fov



MTF comparable to FBP bone
50% lower noise than FBP std
Challenges usual trade-off

IQ	FBP std	FBP bone	MAP-ICD
50% MTF	4.39	8.53	8.66
10% MTF	7.04	11.90	13.20
Std dev	24.99	90.94	13.01

Noise Reduction



Iterative Reconstruction for Multislice Helical Scan CT

64 slice GE VCT



State-of-the-art 3D Recon

GE MBIR
Purdue/Notre Dame/GE algorithm

Iterative Reconstruction for Multislice Helical Scan CT

64 slice GE VCT



State-of-the-art 3D Recon



GE MBIR
Purdue/Notre Dame/GE algorithm

Iterative Reconstruction for Multislice Helical Scan CT

64 slice GE VCT



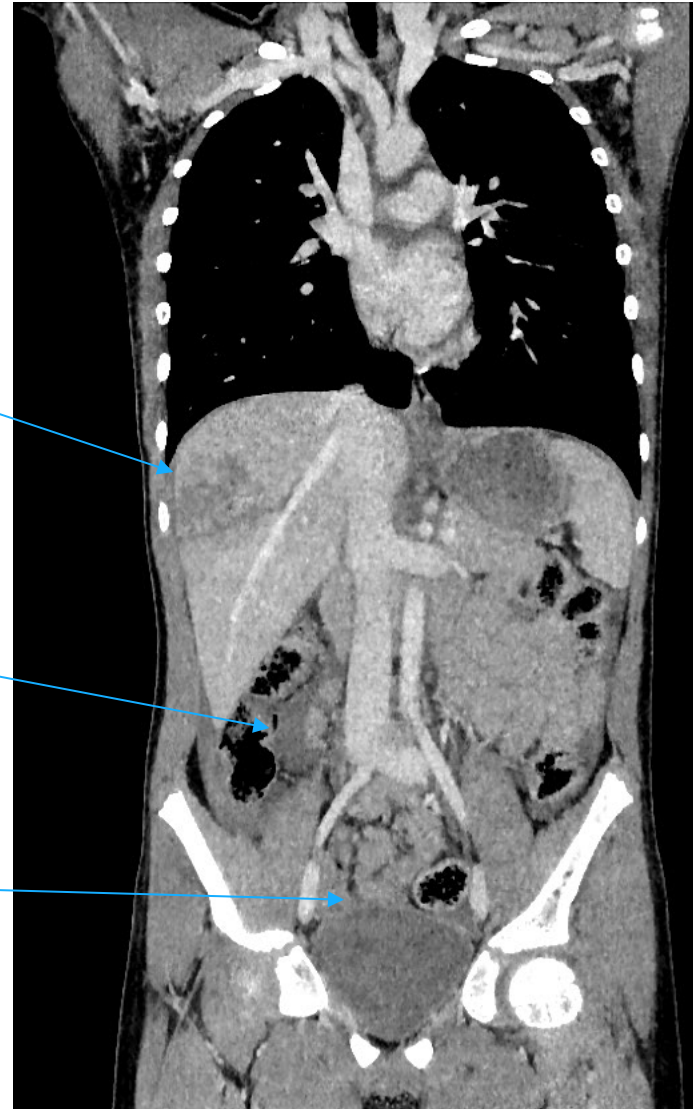
State-of-the-art 3D Recon

GE MBIR
Purdue/Notre Dame/GE algorithm

Pediatric Image at Low Dose (Coronal)



ASiR Reconstruction



Liver laceration better defined

Free fluid/Blood in abdomen seen more clearly

Bladder better visualized

MBIR Reconstruction

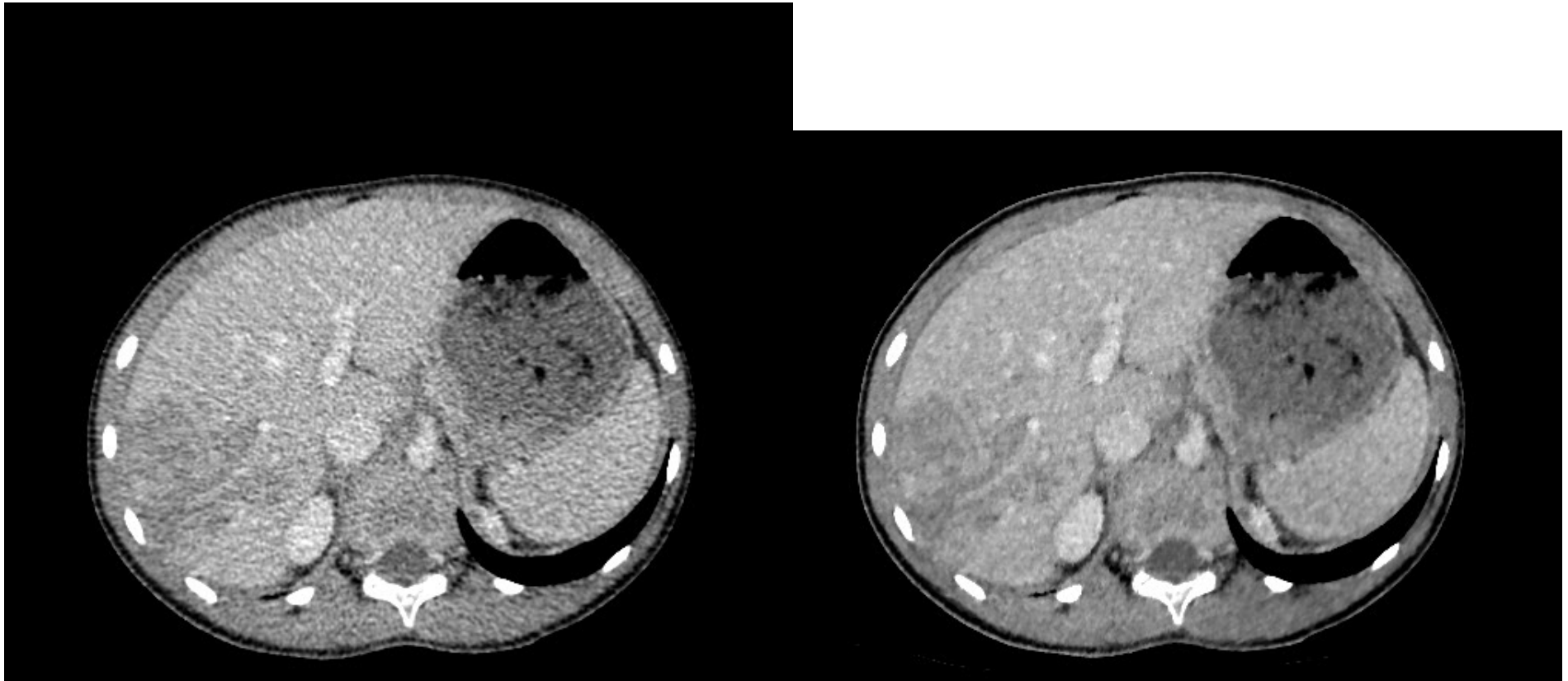
Images courtesy of The Queen Silvia Children's Hospital

Dr. Stålhammar



Pediatric trauma, 120kV, 52-70mA, 0.4s/rot, 0.625mm, WW 300 WL 50

Pediatric Image at Low Dose (Transverse)



ASiR Reconstruction

MBIR Reconstruction

Images courtesy of The Queen Silvia Children's Hospital

Dr. Stålhammar



Pediatric trauma, 120kV, 52-70mA, 0.4s/rot, 0.625mm, WW 300 WL 50

Abdomen Imaging

Adrenal nodule



FBP Reconstruction



MBIR Reconstruction

kV 120, mA 150, 0.5s, 0.625mm, WW 350 WL 50 DFOV 42 Standard kernel in FBP

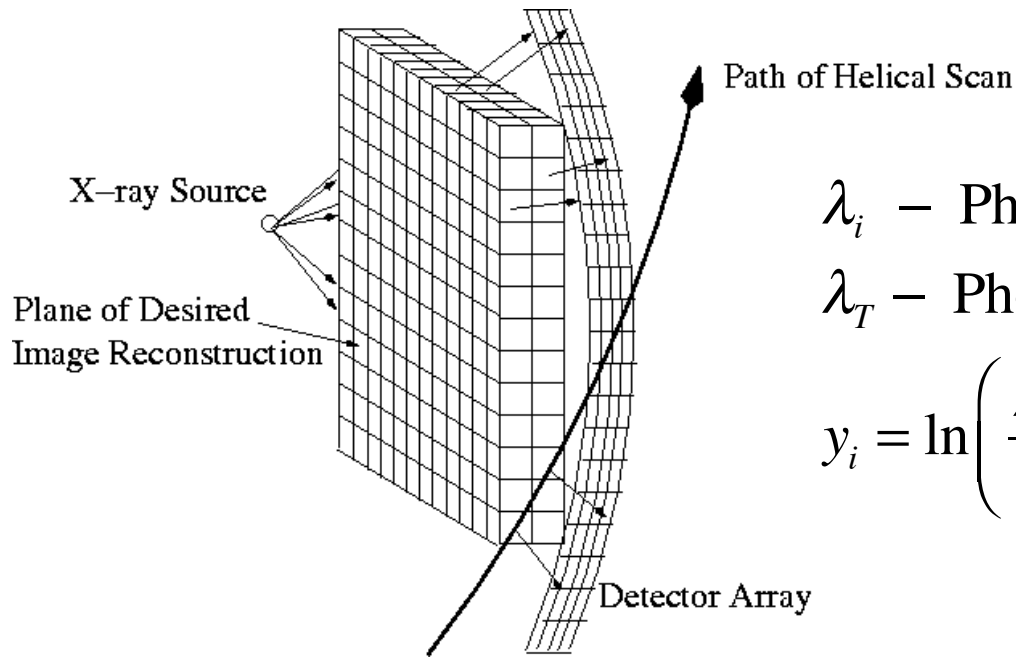
Dual Energy CT

Ruoqiao Zhang, Purdue

Ken Sauer, University of Notre Dame

Jean-Baptiste Thibault, GE Healthcare

Simple Scanner Forward Model: $p(y|x)$



λ_i – Photon count at detector

λ_T – Photon dosage

$y_i = \ln\left(\frac{\lambda_T}{\lambda_i}\right)$ – Attenuation measurement

$$E[y_i | x] = \sum_j A_{i,j} x_j \quad \text{– Line integral through object}$$

$$\text{Var}[y_i | x] \cong \frac{\lambda_i + \sigma_e^2}{\lambda_i^2} \quad \text{– Photon counting + electronic noise}$$

Results in: $-\log p(y|x) = \frac{1}{2} \|y - Ax\|_{\Lambda}^2 + \text{constant}$

Single Energy Transmission Model

- We know that

$$\bar{\lambda}_i = \exp \left\{ - \int_{Ray_i} \mu(e, r) dr \right\}$$

So

$$\bar{y}_i = -\log(\bar{\lambda}_i) = \int_{Ray_i} \mu(e, r) dr$$

■ Conclusions

- At each energy, attenuation is exponential
- $-\log$ of count is proportional to projection of density.
- Produces tomographic reconstruction of densities

Poly-Energetic Transmission Model

- We know that

$$\bar{\lambda}_i = \int_{\mathbb{R}} S(e) \exp \left\{ - \int_{Ray_i} \mu(e, r) dr \right\} de$$

So

$$\bar{y}_i = -\log(\bar{\lambda}_i) = -\log \left(\int_{\mathbb{R}} S(e) \exp \left\{ - \int_{Ray_i} \mu(e, r) dr \right\} de \right) = ??$$

■ Conclusions

- Attenuation is not exponential
- $-\log$ of count is not proportional to projection of density.

Single Material Transmission Model

- Assume that $\mu(e, r) = \mu(e)m(r)$, then

$$\bar{\lambda}_i = \int_{\mathbb{R}} S(e) \exp \left\{ -\mu(e) \int_{Ray_i} m(r) dr \right\} de \quad \begin{array}{l} m(r) : \text{material density} \\ \mu(e) : \text{attenuation} \end{array}$$

So

$$\bar{y}_i = -\log(\bar{\lambda}_i) = h(p_i) \quad \text{or} \quad \hat{p}_i = h^{-1}(y_i)$$

where $h(p) = \int_{\mathbb{R}} S(e) \exp\{-\mu(e)p\} de$ and $p_i = \int_{Ray_i} m(r) dr$

- Conclusions

$h^{-1}(y_i)$ is known as the beam hardening correction

Multiple Material Transmission Model

- Assume that $\mu(e, r) = \mu_1(e)m_1(r) + \mu_2(e)m_2(r)$, then

$$[\bar{y}_{L,i}, \bar{y}_{h,i}] = \left[-\log(\bar{\lambda}_{L,i}), -\log(\bar{\lambda}_{L,i}) \right] = h(p_{1,i}, p_{2,i})$$

$$[p_1, p_2] = \int_{Ray_i} [m_1(r), m_2(r)] dr$$

$[m_1(r), m_2(r)]$: material densities for water and iodine

$[\mu_1(e), \mu_2(e)]$: mass attenuation function for water and iodine

where

$$h(p_1, p_2) = -\log \left(\int_{\mathbb{R}} [S_1(e), S_2(e)] \exp\{-\mu_1(e)p_1 - \mu_2(e)p_2\} de \right)$$

- Conclusions

$h^{-1}(y_{l,i}, y_{h,i})$ is known as the material decomposition function

Dual Energy CT

- Make transmission measurement

$$[\bar{y}_{l,i}, \bar{y}_{h,i}] = \left[-\log(\bar{\lambda}_{l,i}), -\log(\bar{\lambda}_{h,i}) \right] = h(p_{1,i}, p_{2,i})$$

- For FBP, perform material decomposition

$$h^{-1}(\bar{y}_{l,i}, \bar{y}_{h,i}) = [p_{1,i}, p_{2,i}] = \int_{Ray_i} [m_1(r), m_2(r)] dr$$

- But for MBIR, the forward model is

$$[\bar{y}_{l,i}, \bar{y}_{h,i}] = h(p_{1,i}, p_{2,i})$$

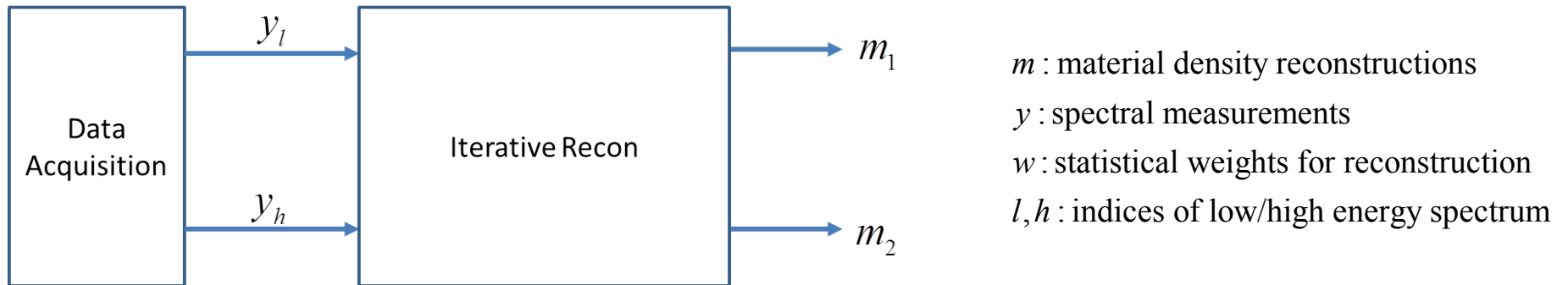
which leads to

$$-\log p(y|m) = \frac{1}{2} \sum_i \begin{bmatrix} y_{l,i} - h_l(p_{1,i}), & y_{h,i} - h_h(p_{2,i}) \end{bmatrix} \begin{bmatrix} w_l & 0 \\ 0 & w_h \end{bmatrix} \begin{bmatrix} y_{l,i} - h_l(p_{1,i}) \\ y_{h,i} - h_h(p_{2,i}) \end{bmatrix}$$

Approach I: Full Nonlinear Inversion

- Nonlinear inversion from spectral measurements to material densities.

(TIP 2009 O'Sullivan and Benac) (ISBI 2009 Huh and Fessler)



$$\hat{m} = \arg \min_m \left\{ \frac{1}{2} \sum_i \left[\begin{array}{c} y_{l,i} - h_l(A_{i,*}, m_1) \\ y_{h,i} - h_h(A_{i,*}, m_2) \end{array} \right] \left[\begin{array}{cc} w_l & 0 \\ 0 & w_h \end{array} \right] \left[\begin{array}{c} y_{l,i} - h_l(A_{i,*}, m_1) \\ y_{h,i} - h_h(A_{i,*}, m_2) \end{array} \right] + S(m) \right\}$$

- Pros:

- High flexibility;
- Can achieve high model accuracy.

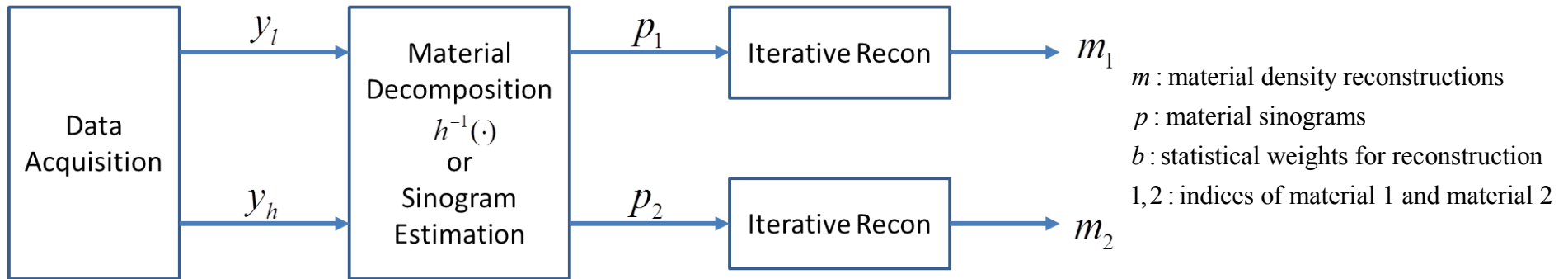
- Cons:

- Complex forward model, computationally difficult to model during iterations.

Approach II: Linearized Model w/ Diagonal Weighting

- Work from material sinograms to reconstruct each material individually.

(NSS 2004 Kinahan and Fessler)



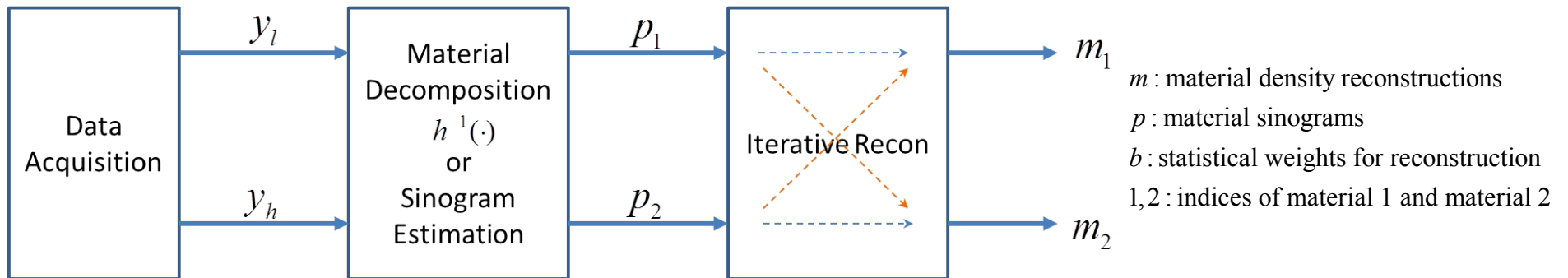
$$\begin{bmatrix} \hat{p}_{1,i} \\ \hat{p}_{2,i} \end{bmatrix} = h^{-1}(y_{l,i}, y_{h,i})$$

$$\hat{m} = \arg \min_m \left\{ \frac{1}{2} \sum_i \begin{bmatrix} \hat{p}_{l,i} - A_{i,*} m_1 & \hat{p}_{h,i} - A_{i,*} m_2 \end{bmatrix} \begin{bmatrix} b_1 & 0 \\ 0 & b_2 \end{bmatrix} \begin{bmatrix} \hat{p}_{l,i} - A_{i,*} m_1 \\ \hat{p}_{h,i} - A_{i,*} m_2 \end{bmatrix} + (S(m_1) + S(m_2)) \right\}$$

- Pros:
 - Simpler forward model; computationally more practical.
- Cons:
 - Does not account for the well-known correlation between different material sinograms; (TMI'88 Kalender, Klotz and Kostaridou).

Proposed: Model with Full Statistical Weighting

- Models the interdependency between different materials.



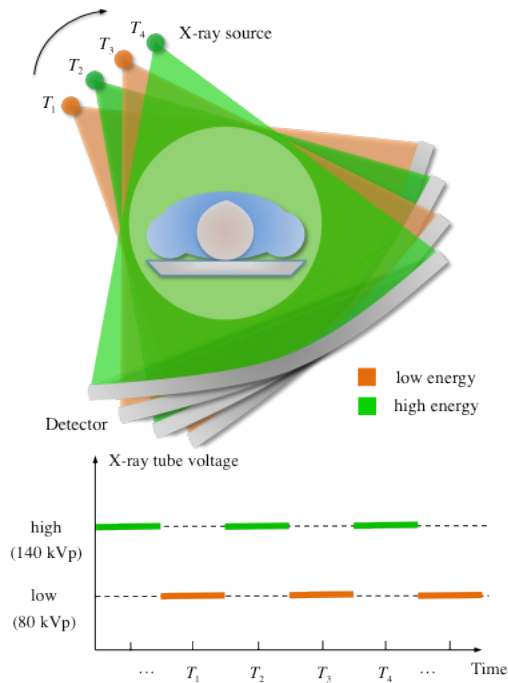
$$\begin{bmatrix} \hat{p}_{1,i} \\ \hat{p}_{2,i} \end{bmatrix} = h^{-1}(y_{l,i}, y_{h,i})$$

$$\hat{m} = \arg \min_m \left\{ \frac{1}{2} \sum_{\text{rays}} \begin{bmatrix} \hat{p}_{l,i} - A_{i,*} m_1 \\ \hat{p}_{h,i} - A_{i,*} m_2 \end{bmatrix} \begin{bmatrix} b_1 & b_3 \\ b_3 & b_2 \end{bmatrix} \begin{bmatrix} \hat{p}_{l,i} - A_{i,*} m_1 \\ \hat{p}_{h,i} - A_{i,*} m_2 \end{bmatrix} + (S(m_1) + S(m_2)) \right\}$$

- Off-diagonal weights model the correlation between p_1 and p_2 .

$$B \triangleq \begin{bmatrix} b_1 & b_3 \\ b_3 & b_2 \end{bmatrix} = \left[\nabla h^{-1}(y) \right]^{-1} \begin{bmatrix} w_l & 0 \\ 0 & w_h \end{bmatrix} \left[\nabla h^{-1}(y) \right]^{-T}$$

Fast kV Switching



- Alternating samples from high and low energy source
- Samples are missing!
- Solution: Interpolate missing sample, but use zero weighting

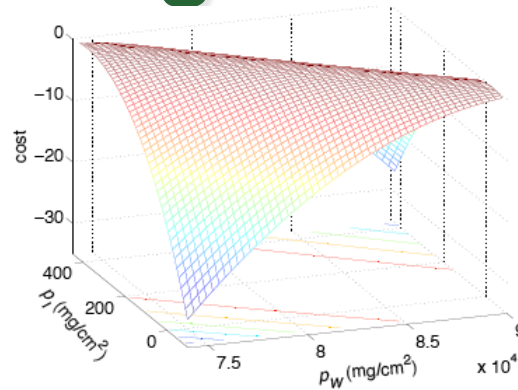
If low kV, then =>

$$B = \left[\nabla h^{-1}(y) \right]^{-1} \begin{bmatrix} w_l & 0 \\ 0 & 0 \end{bmatrix} \left[\nabla h^{-1}(y) \right]^{-T}$$

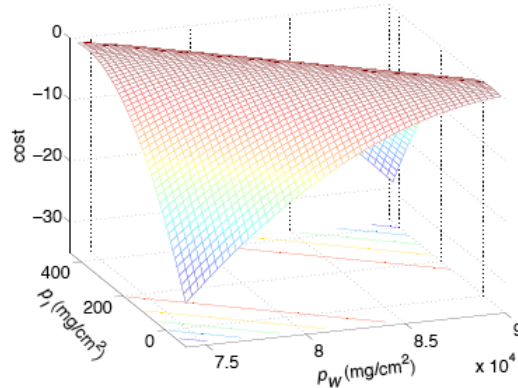
If high kV, then =>

$$B = \left[\nabla h^{-1}(y) \right]^{-1} \begin{bmatrix} 0 & 0 \\ 0 & w_h \end{bmatrix} \left[\nabla h^{-1}(y) \right]^{-T}$$

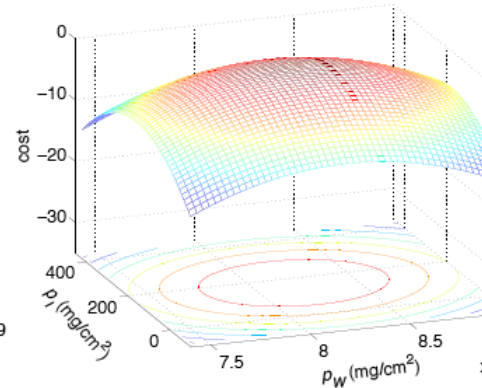
Important of Diagonal Terms in Fast kV Switching



(a) true log-likelihood



(b) joint approximation



(c) independent approximation

- Joint log-likelihood approximation is insensitive to interpolated value!

Non-negativity for Dual Energy Optimization

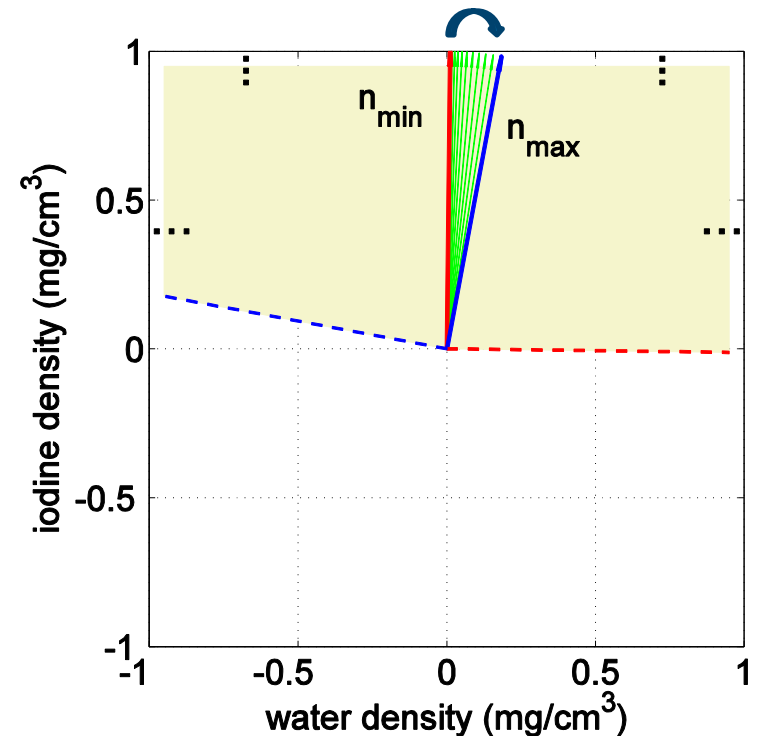
Infinite number of constraints:

$$\Omega = \left\{ (m_1, m_2) : \mu_1(e) m_1 + \mu_2(e) m_2 \geq 0, \forall e \in [40, 140] \text{keV} \right\}$$



Two constraints:

$$\left\{ m = (m_1, m_2) : m \cdot n_{\min}^T \geq 0 \text{ and } m \cdot n_{\max}^T \geq 0 \right\}.$$



Experiments

- We compare three DECT reconstruction methods:

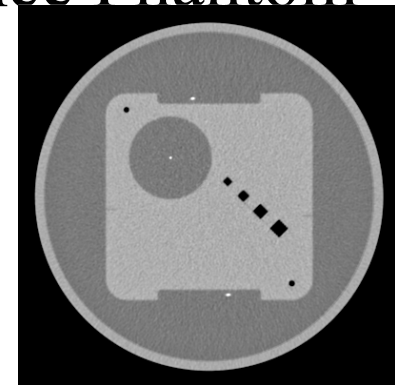
1. Denoised FBP;
2. Incomplete DE-MBIR;
3. Joint DE-MBIR.

$$\Rightarrow B = \begin{bmatrix} b_1 & 0 \\ 0 & b_2 \end{bmatrix}$$

$$\Rightarrow B = \begin{bmatrix} b_1 & b_3 \\ b_3 & b_2 \end{bmatrix}, b_3 \neq 0$$

- Phantom recon with the GE Performance Phantom

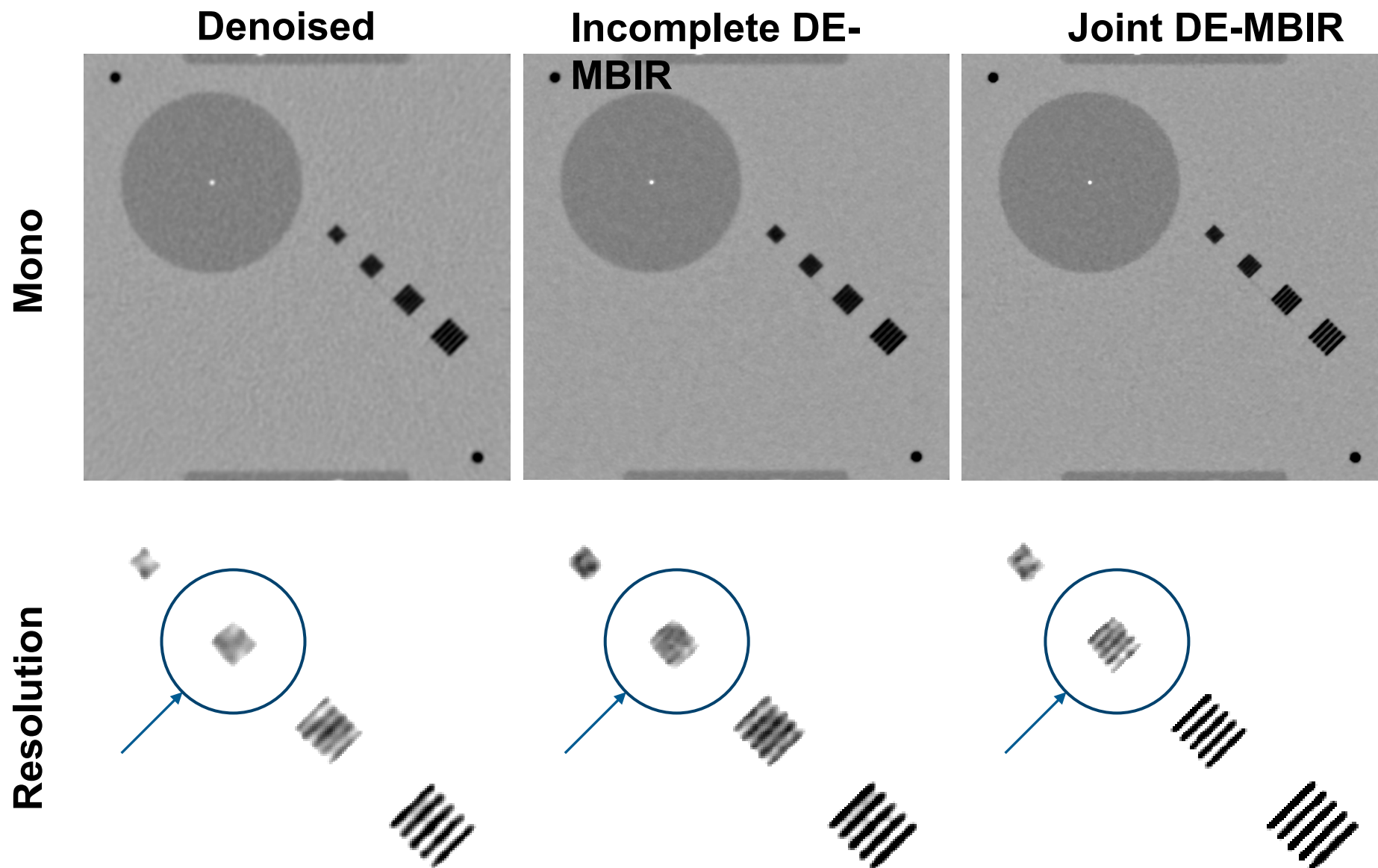
- Qualitative comparison;
- Noise level evaluation;
- Resolution evaluation.



- Clinical recon with a GSI abdominal scan

- Qualitative comparison.

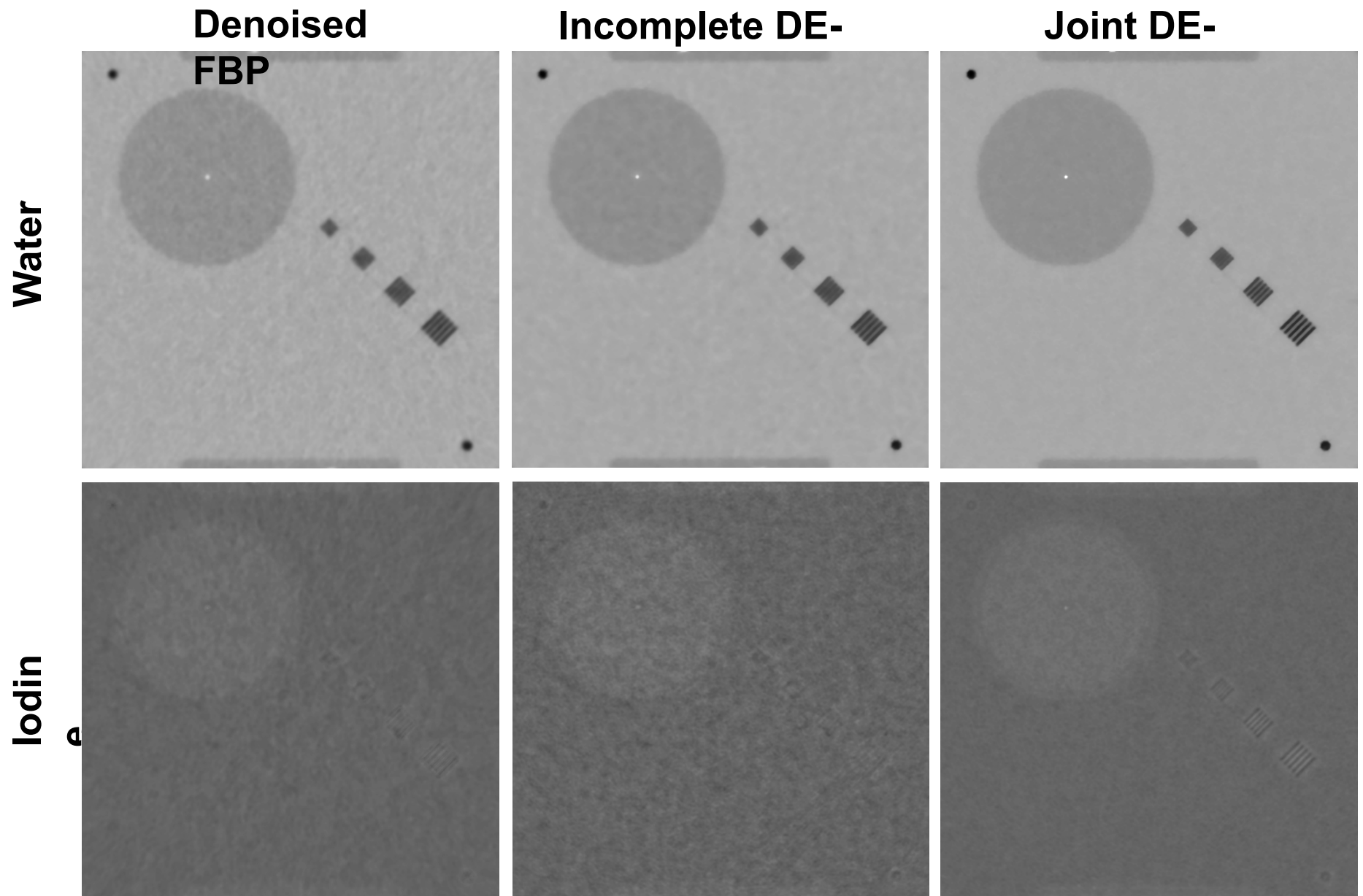
Phantom Results: Monochromatic at 70keV



mono: WL 0HU, WW1000HU;

resolution bars: WL 600HU, WW 200HU.

Phantom Results: Water and Iodine

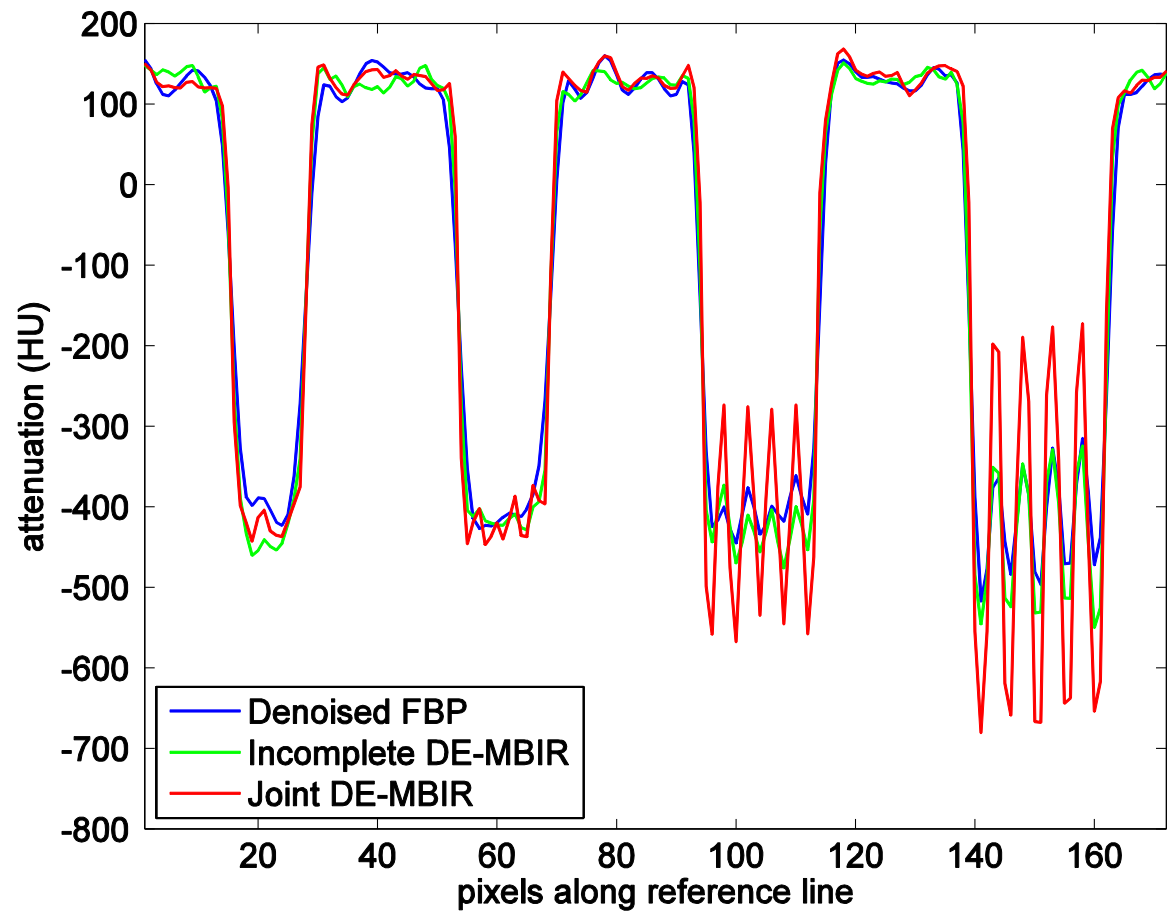
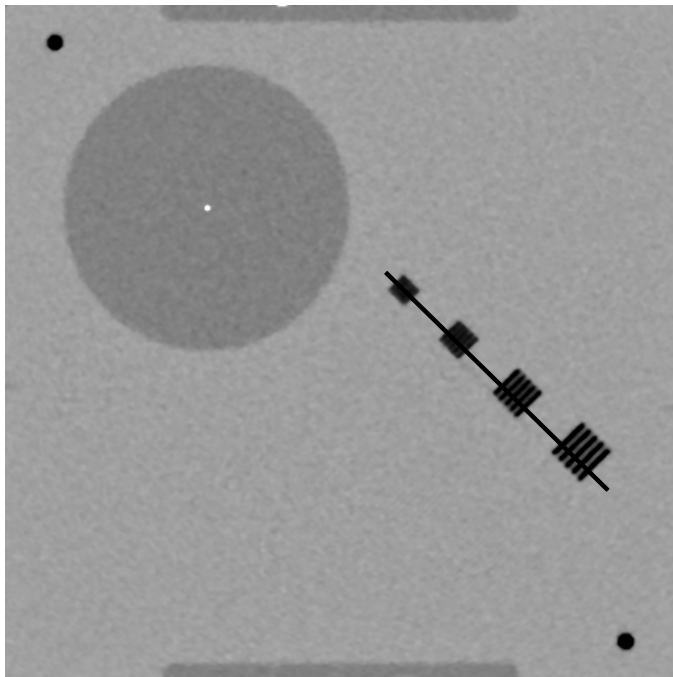


water: WL 900mg/cc, WW1600mg/cc;

iodine: WL 3mg/cc, WW 40mg/cc.

Phantom Results: Resolution Bars

- CT values in the 70keV attenuation map along reference line.



Evaluation Metrics

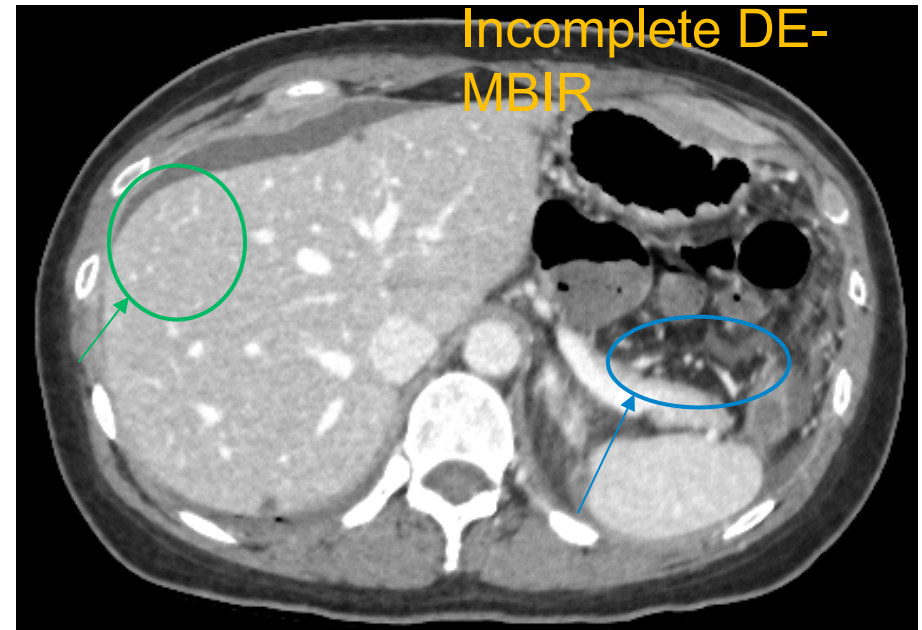
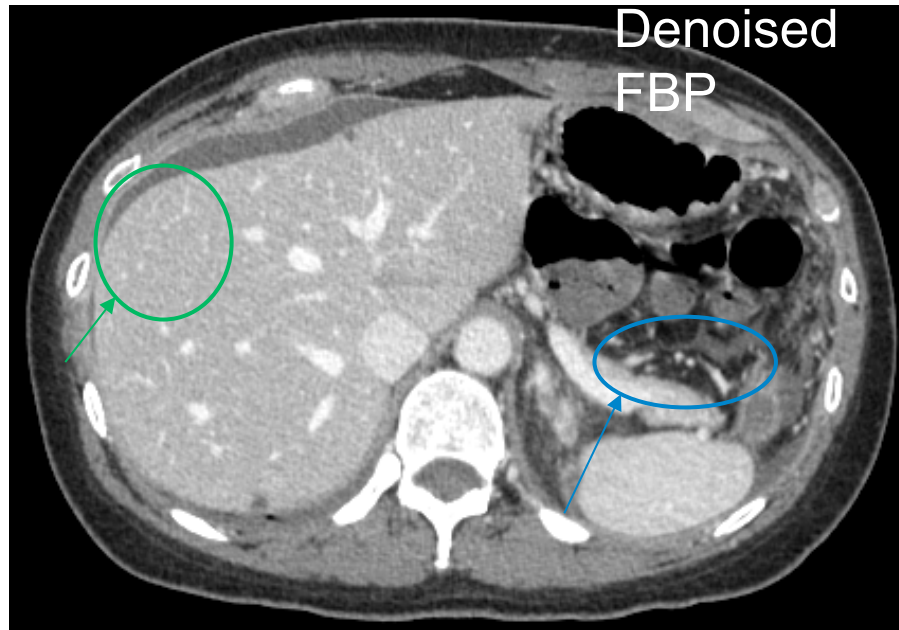
	Noise Std. Dev.			10% MTF (lp/cm) *		
	Water (mg/cc)	Iodine (mg/cc)	Mono (HU)	Water	Iodine	Mono
Denoised FBP	21.21	0.60	14.18	6.15	5.81	6.60
Incomplete DE-MBIR	14.31	0.89	13.55	8.61	6.35	8.90
Joint DE-MBIR	9.68	0.30	13.69	11.80	10.59	11.70

■ **Conclusions:**

With comparable noise level in 70keV monochromatic images

1. Joint DE-MBIR significantly reduces noise compared to FBP and Incomplete DE-MBIR in material density images.
2. Joint DE-MBIR improves overall in-plane resolution by roughly 90% over FBP, and 40% over Incomplete DE-MBIR.

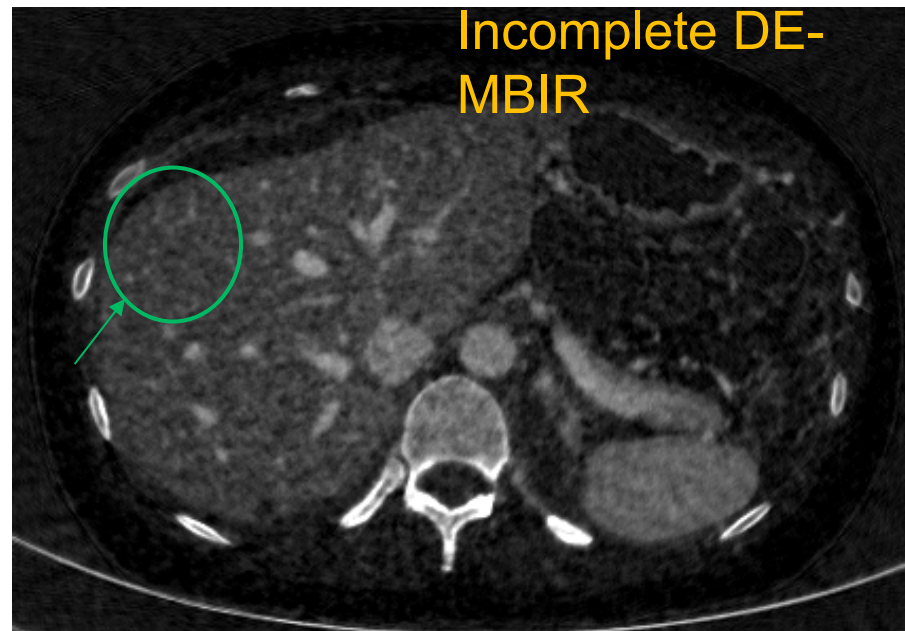
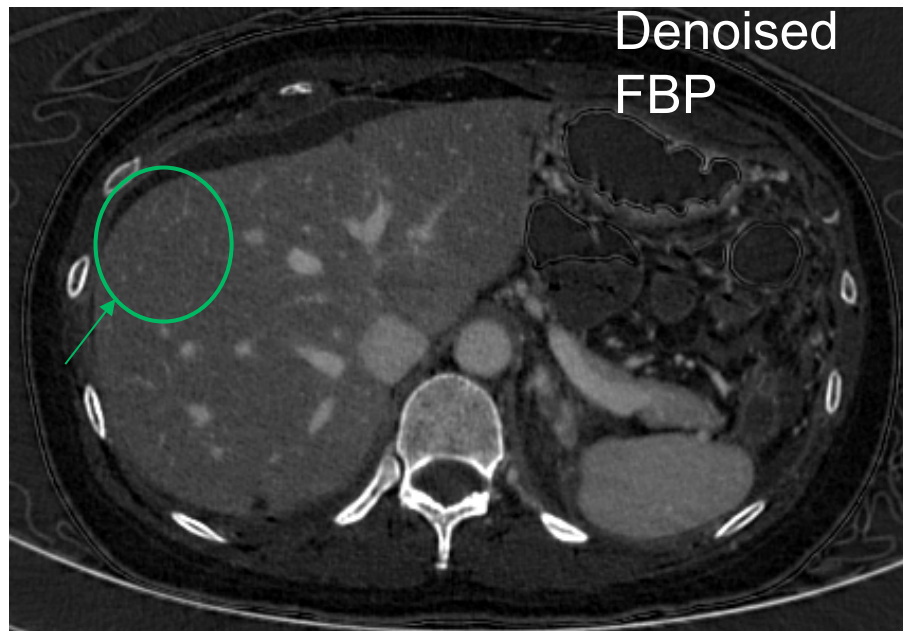
Clinical Results: Monochromatic at 70keV



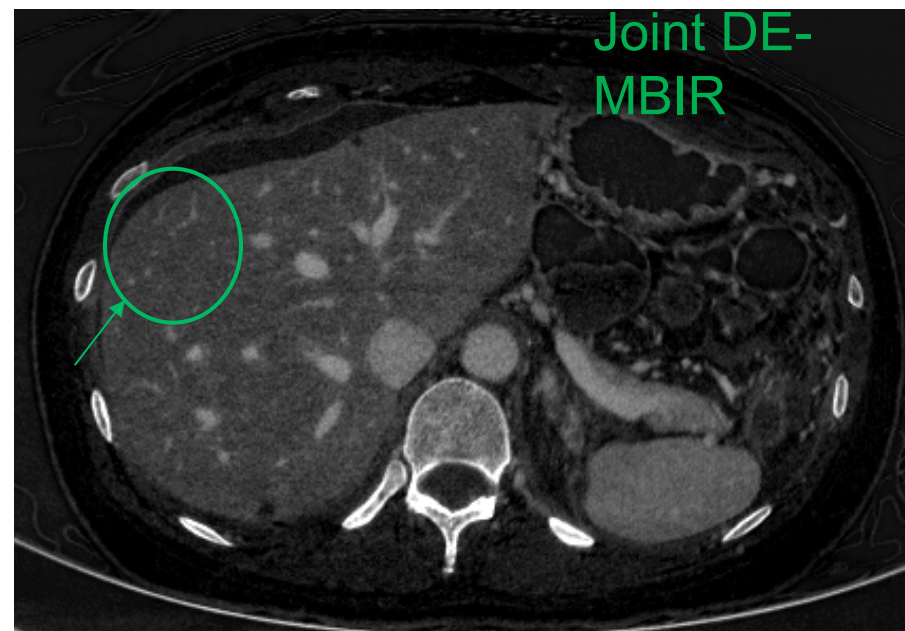
- Joint DE-MBIR achieves:
 - resolution improvement
 - contrast improvement

* matched noise level in mono images

Clinical Results: Iodine

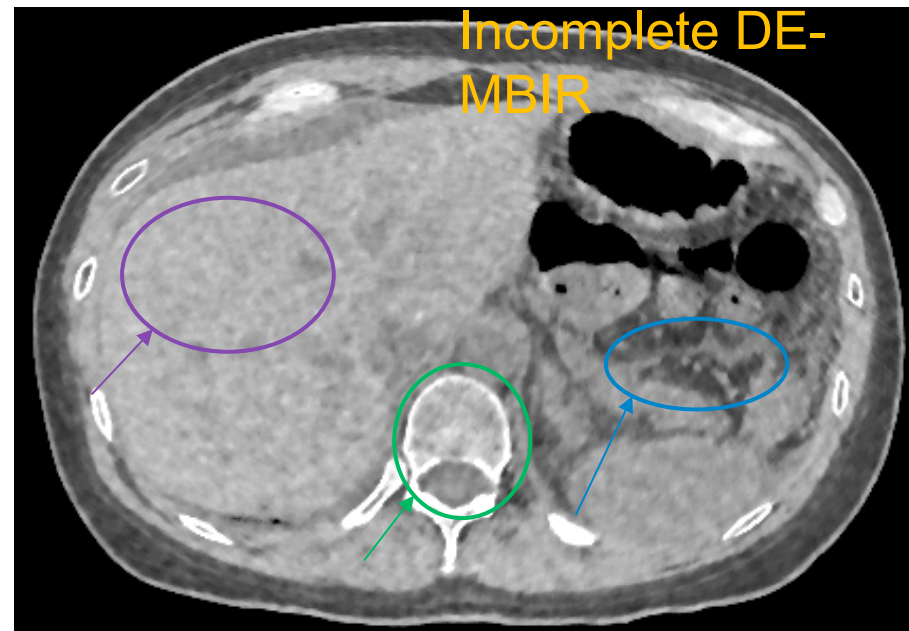
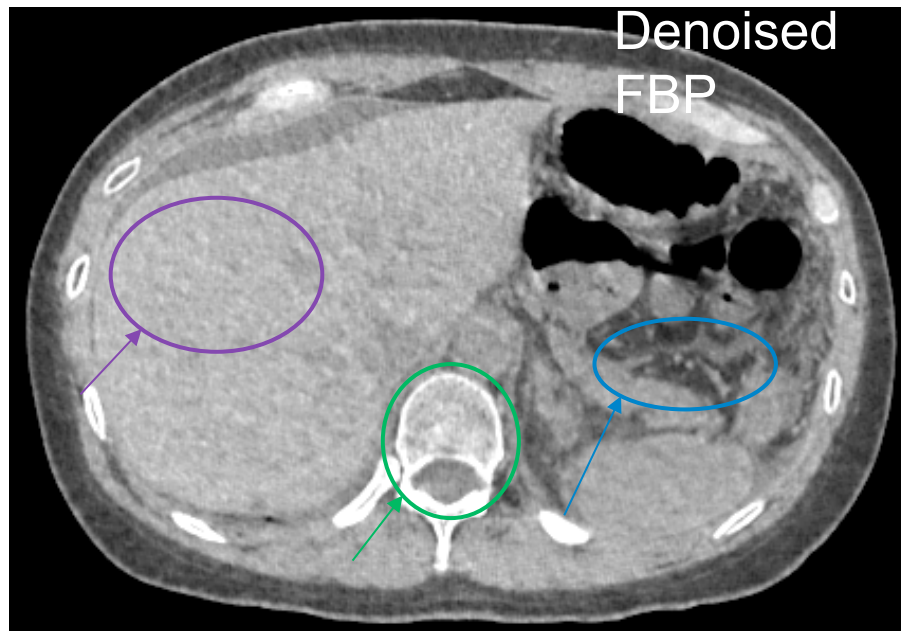


- Joint DE-MBIR achieves:
 - **contrast improvement**

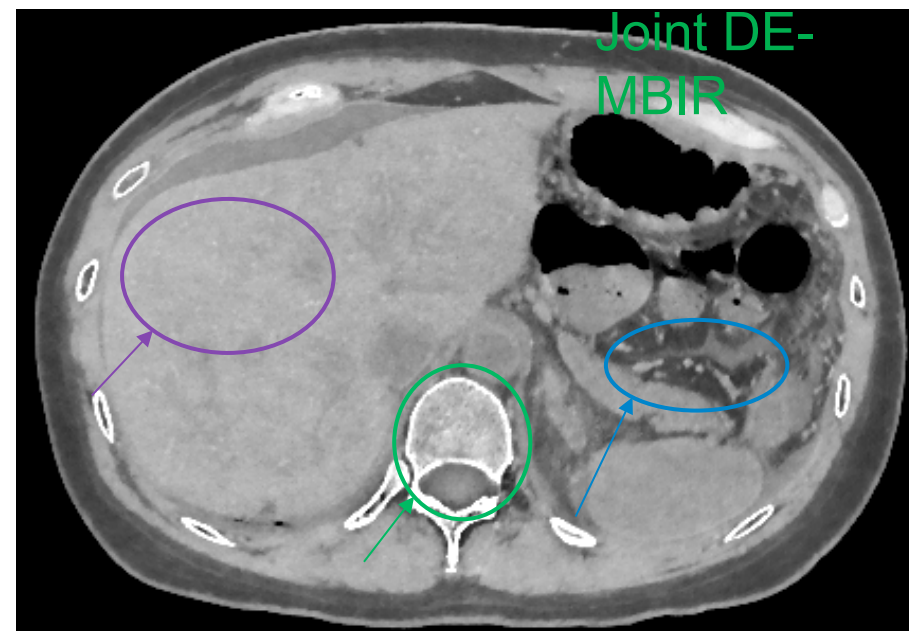


* matched noise level in mono images

Clinical Results: Water



- Joint DE-MBIR achieves:
 - resolution improvement
 - noise reduction
 - bone improvement



* matched noise level in mono images

Security Imaging

Sondre Skatter, Morpho Detection

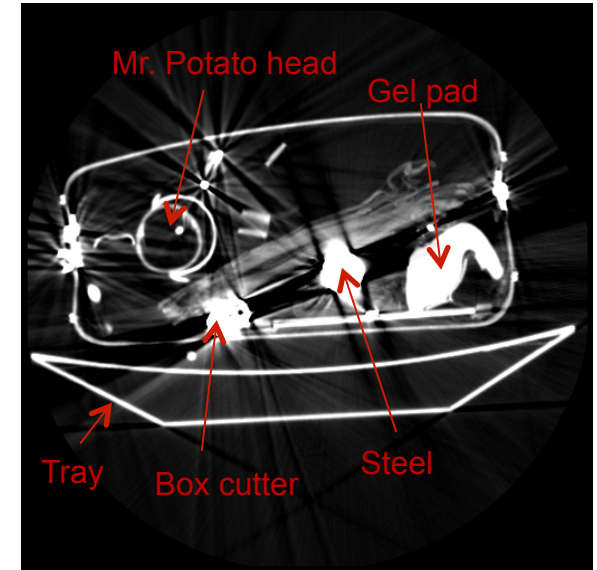
Simon Bedford, Astrophysics

Jordan Kisner, Purdue

Eri Haneda, Purdue

Why could MBIR be valuable in Security Applications?

- Reduced artifacts
 - Reduction of streaks => Better segmentation
 - Reduced metal artifacts
 - Reduced beam-hardening artifacts
- Reconstruction from non-classical measurements
 - Limited angle/limited view
 - Fixed gantry systems
 - Multimodal/nonlinear measurements
 - Dual or poly-energetic
 - Integrated projection/scatter from active/passive sources
- Incorporation of more physical real-world constraints
 - Material characteristic
 - Image structure
 - Integrated reconstruction and processing (reconstruction and segmentation)



FBP reconstruction

Microscopy for Material Science

Venkat Venkatakrisnan, Purdue

Larry Drummy, AFRL

Marc De Graef, CMU

Jeff Simmons, AFRL

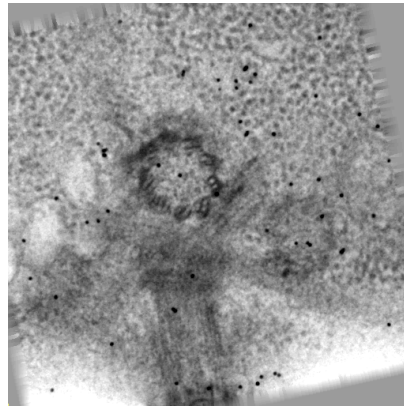
Electron Microscopy Imaging

- 2-D Characterization of samples (biology, material science)
- Various modalities (Bright Field, Dark Field etc.)

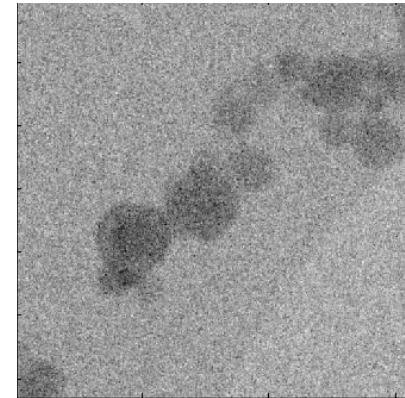


STEM

Bright Field

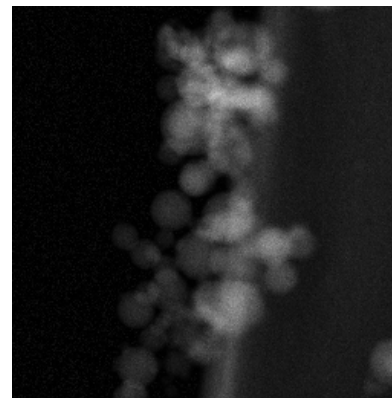


Biological sample*



Aluminum nanoparticles**

Dark Field

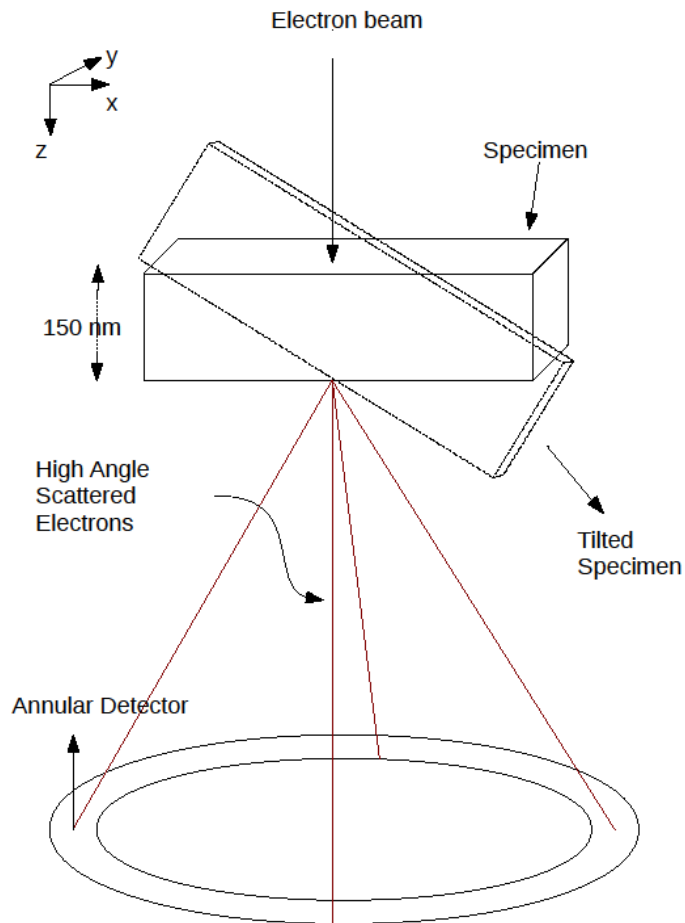


Aluminum nanoparticles**

*<http://bio3d.colorado.edu/imod/doc/etomoTutorial.html>

** L.F. Drummy, AFRL

High Angle Annular Dark Field (HAADF) STEM Tomography



■ Acquisition

- An electron beam is focused at a point on the sample.
- An annular ring detects elastically scattered electrons, but angle is small.

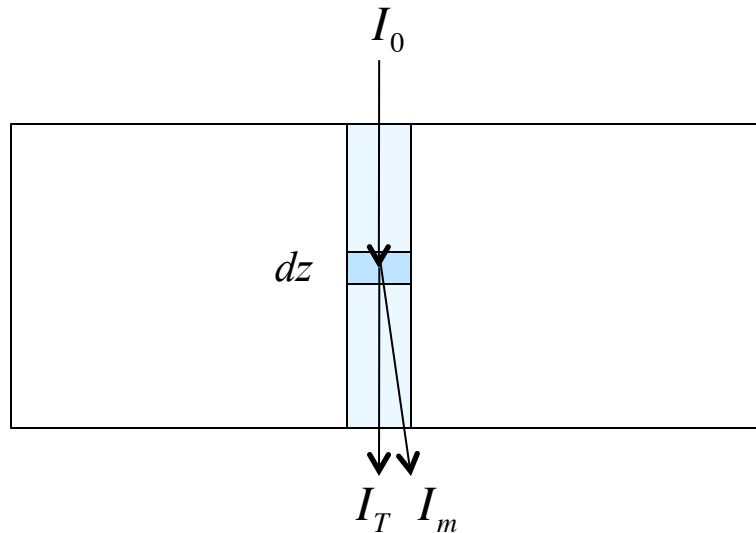
■ Geometry

- Electron beam is scanned across sample
- Sample is tilted in one axis
- Results in 2D parallel beam data

■ Forward model

- Dark field => emission equations
- Bright field => transmission equations

HAADF and BF Measurement Models



Scattering coefficient:

$$s(z) = \sigma(z)N(z)$$

Attenuation coefficient:

$$\mu(z)$$

Attenuation of unscattered beam

$$I(z) = I_0 \exp\left(-\int_0^z \mu(r) dr\right)$$

$$I_T \triangleq I(z)$$

Attenuation of scattered beam

$$\frac{dI_m}{dz} = I(z)s(z)$$

$$I_m = \int_0^T I(z)s(z) dz \cong I_0 \int_0^T s(z) dz$$

So we get

$$\int_0^T s(z) dz = \frac{I_m}{I_0}$$
$$\int_0^T \mu(z) dz = -\log\left(\frac{I_T}{I_0}\right)$$

MAP Cost Function for HAADF Problem

- MAP cost function is given by

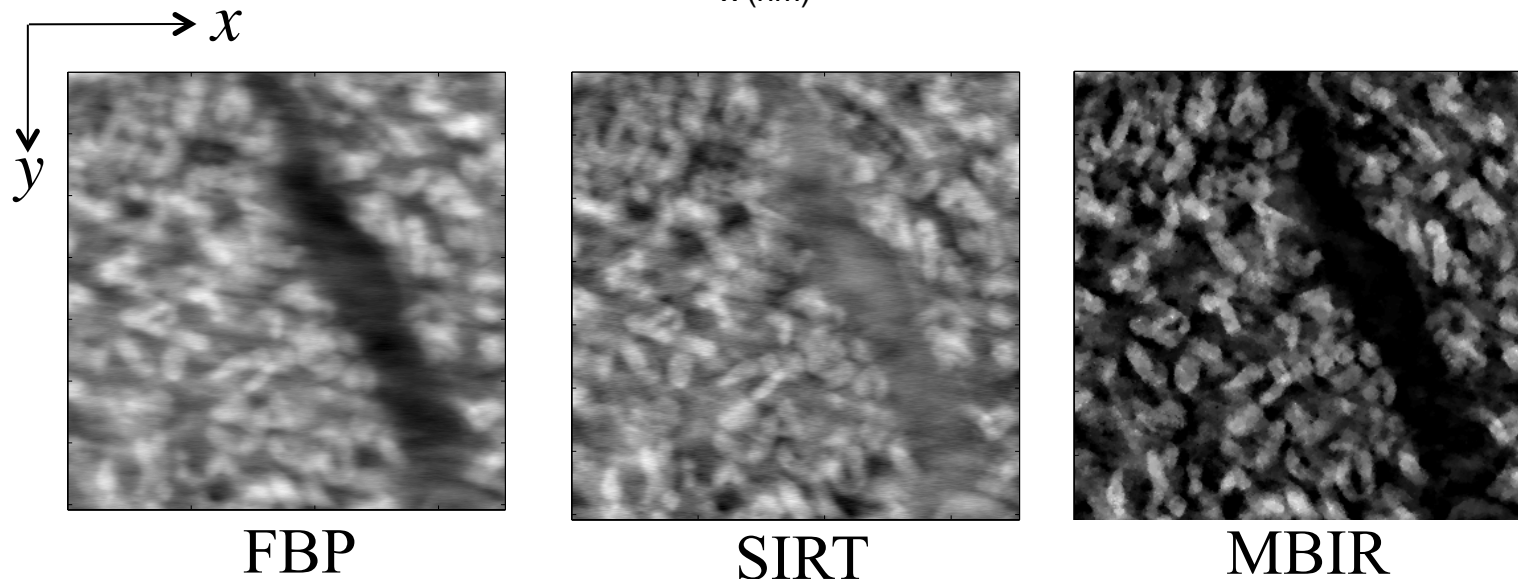
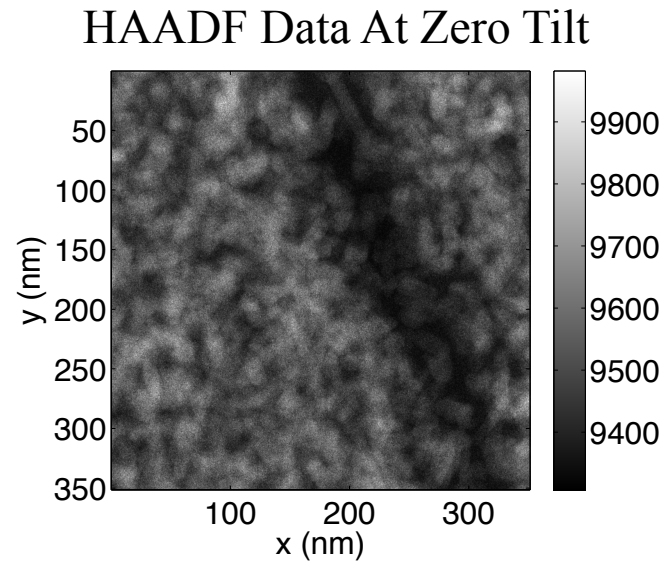
$$\hat{x} = \arg \min_{x \geq 0} \min_{I, \mu} \left\{ \sum_{k=0}^{N_v-1} \frac{1}{2} \|y_k - I_{0,k} A_k x - \mu_k \mathbf{1}\|_{\Lambda_k}^2 + \frac{1}{p \sigma_x^p} \sum_{\{i,j\} \in \zeta} w_{ij} |x_i - x_j|^p \right\}$$

$$\text{subject to the constraint } \prod_{k=0}^{N_v-1} I_k = \bar{I}_0$$

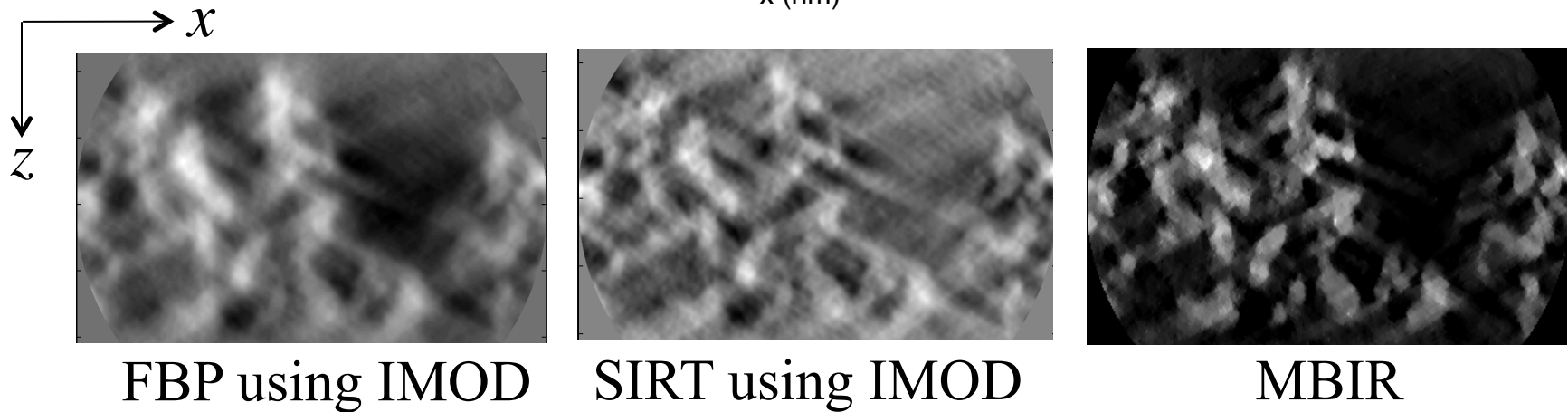
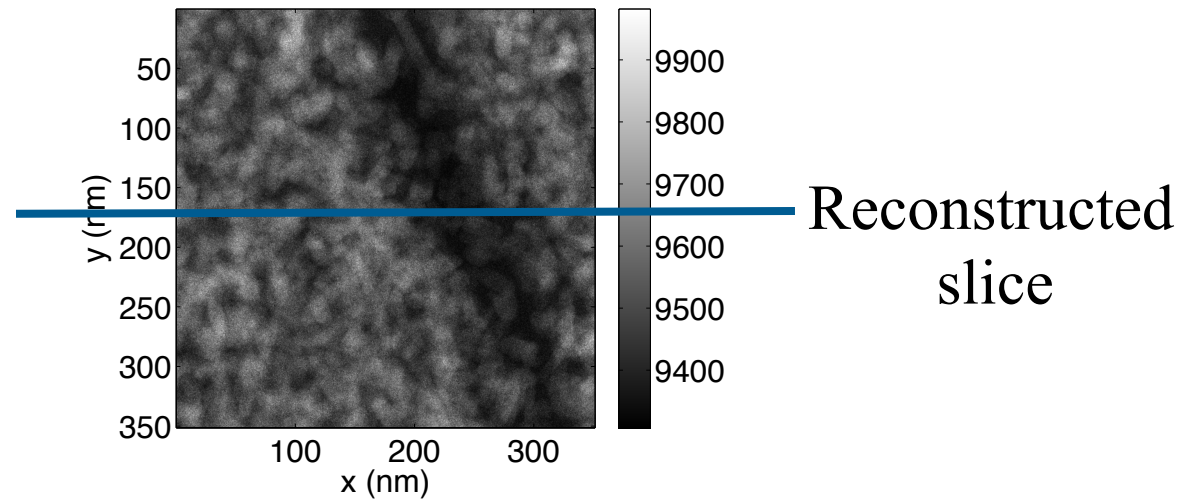
Model-based reconstruction allows use to estimate unknown parameters for offset, gain and noise.

Titanium Dioxide Nanoparticle* (x-y slice)

- Polystyrene functionalized titanium dioxide nanoparticles
- 87 tilts from -70° to $+70^\circ$



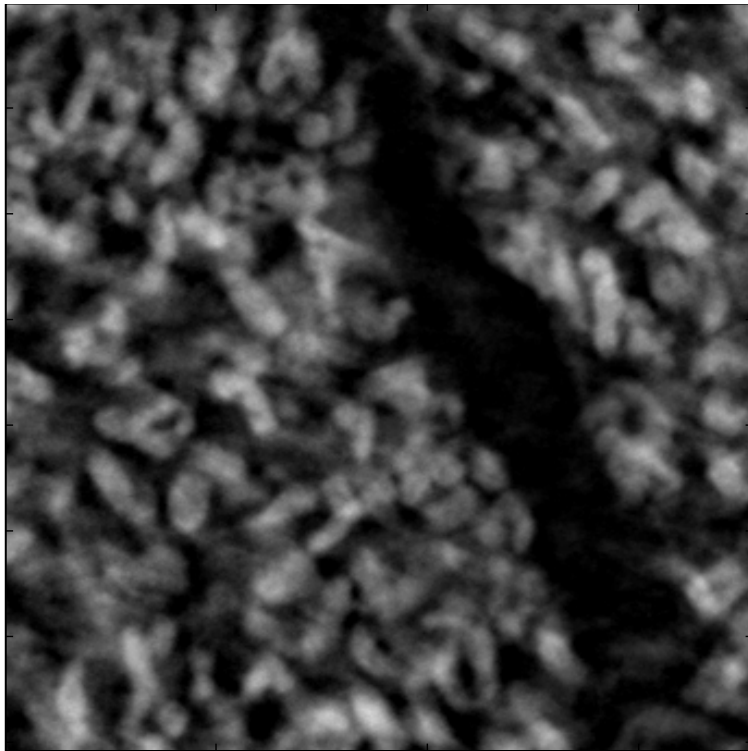
3-D Reconstruction (x-z slice)



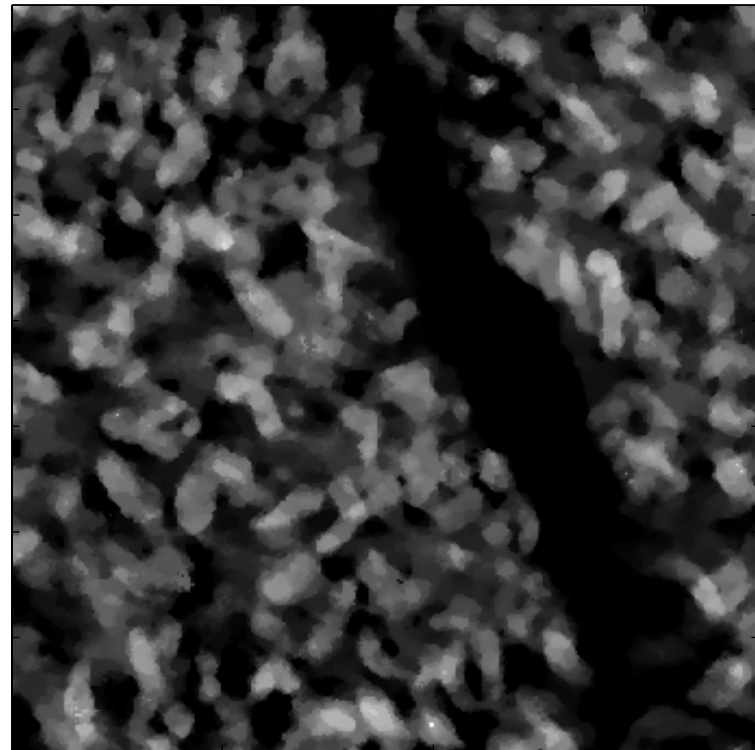
3-D Reconstruction (x-y slice)

Impact of varying p in prior

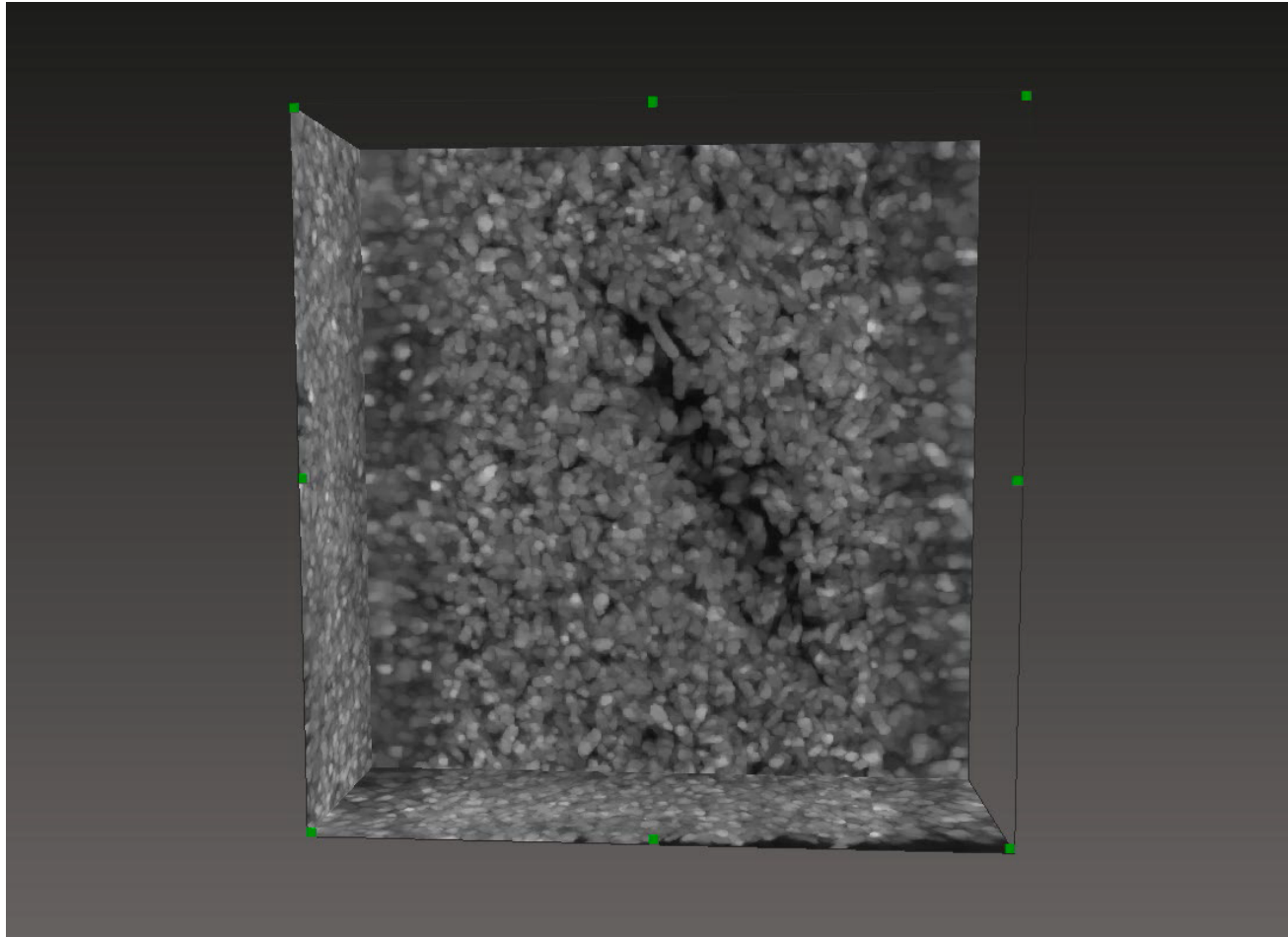
$p = 2$



$p = 1$



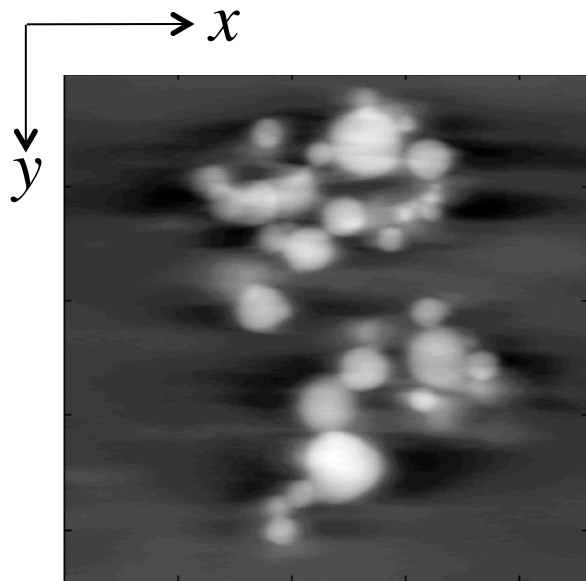
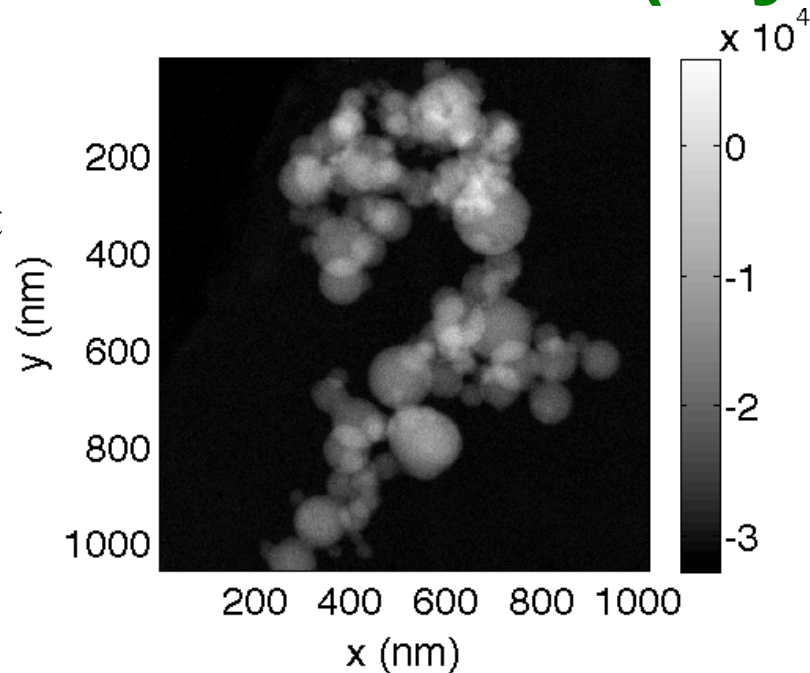
TiO₂ Reconstruction 3D Rendering*



*Lawrence Drummy, AFRL

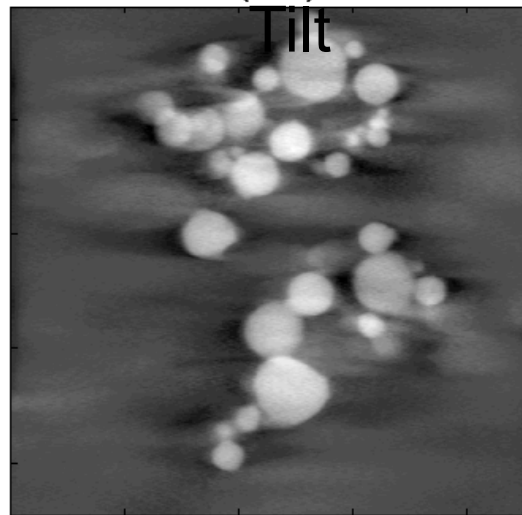
Real Al Sphere Data Set* (x-y slice)

- Aluminum spheres in a carbon support (600 nm thick)
- 65 tilts from -70° to $+70^\circ$

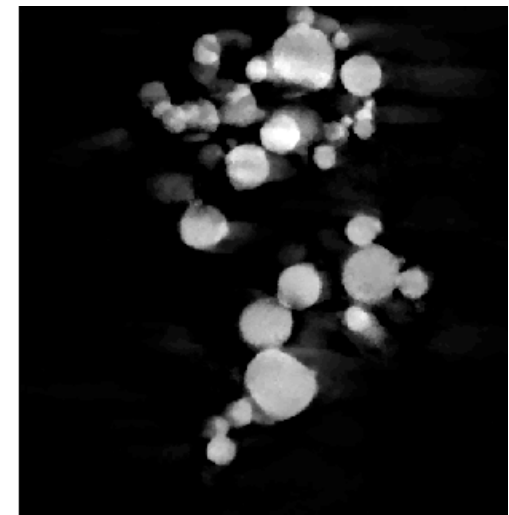


FBP using IMOD

**Lawrence Drummy, AFRL*

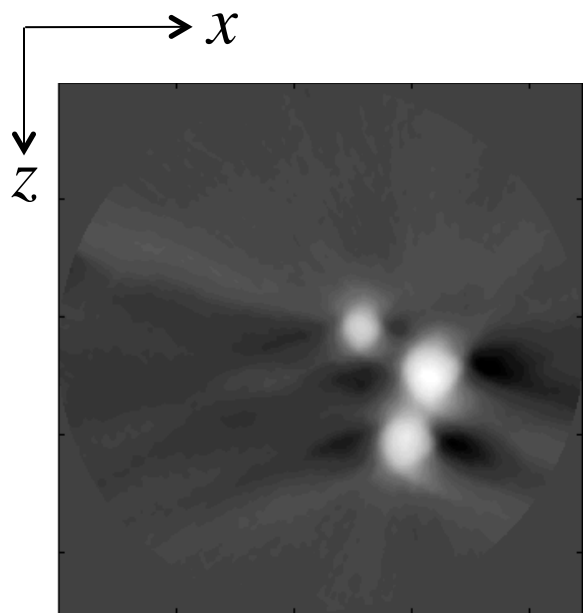
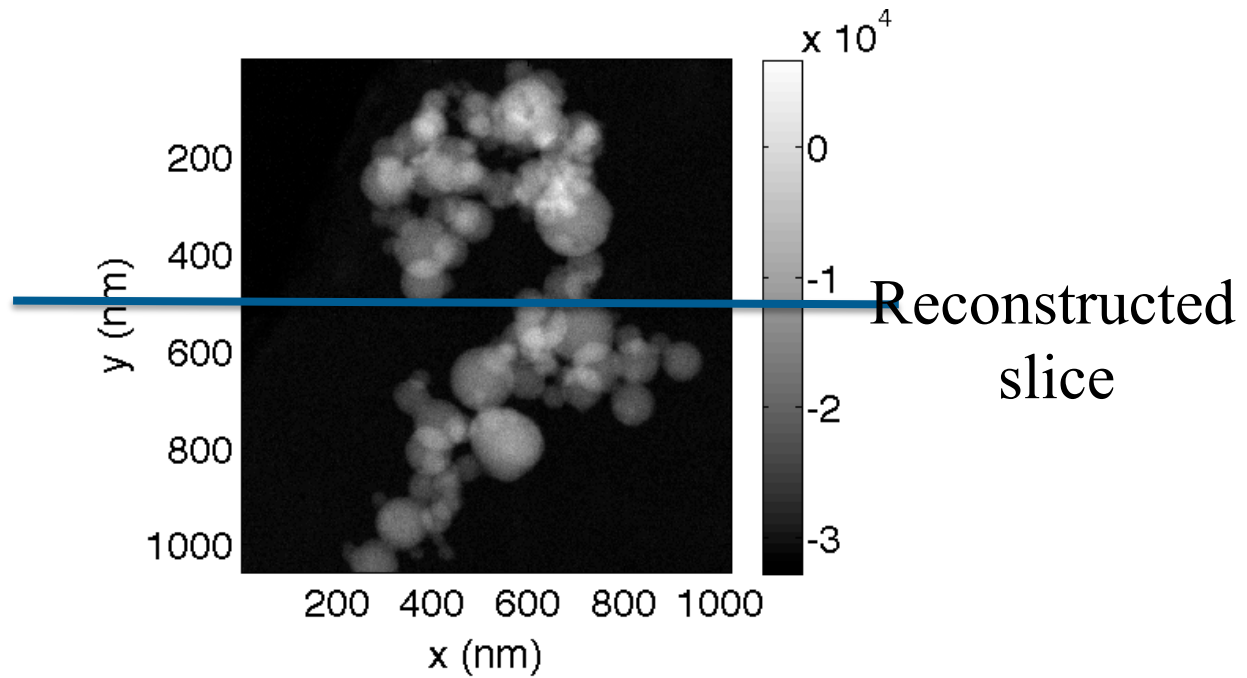


SIRT using IMOD

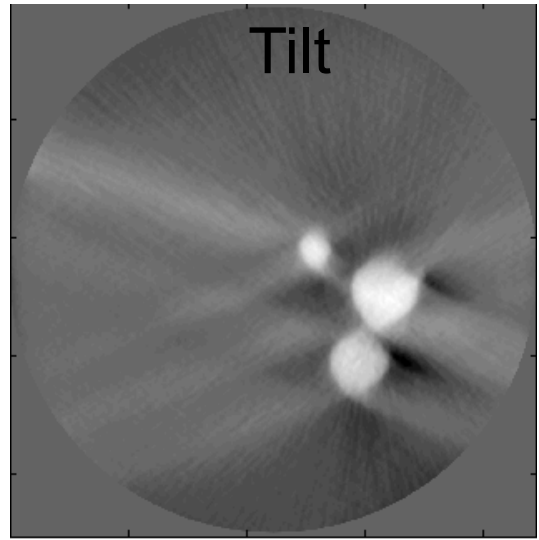


MBIR

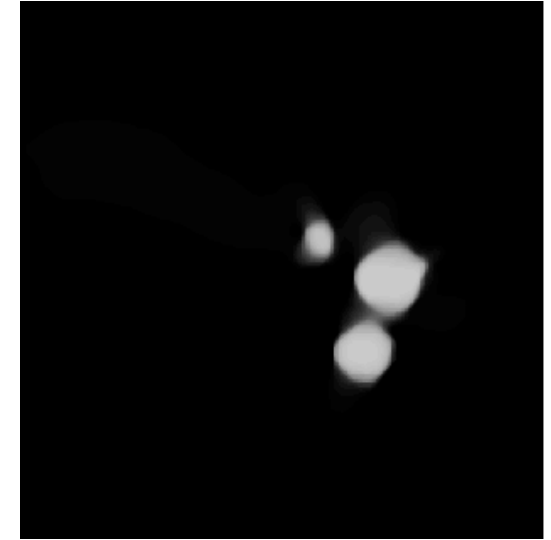
Real Al Spheres (x-z slice)



FBP using IMOD



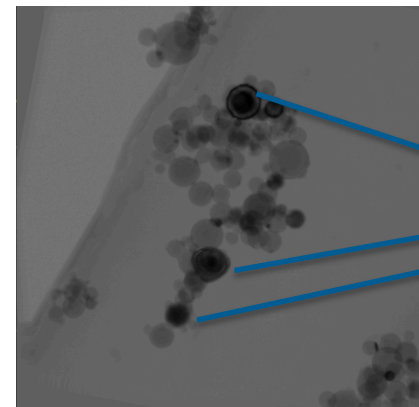
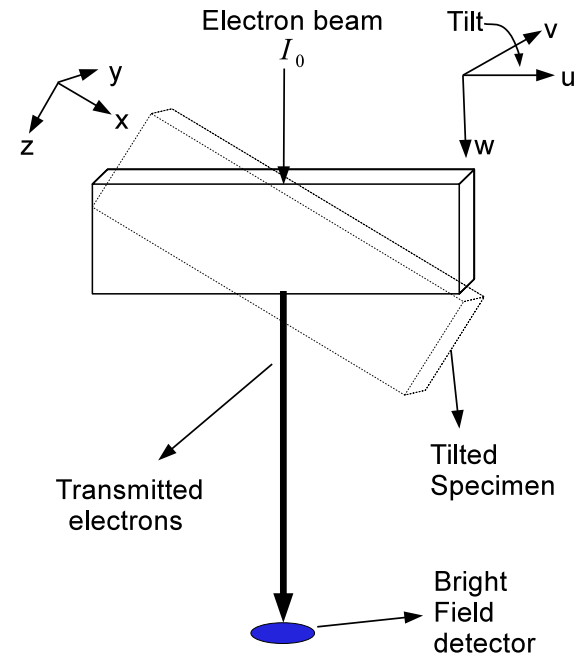
SIRT using IMOD



MBIR

Bright Field (BF) Electron Tomography

- Problem: 3-D reconstruction of BF images is normally not done due to anomalous effects of Bragg scatter.
- Medium term approach: Detect Bragg scatter as part of the reconstruction process forward modeling.
- Long term approach: Model Bragg scatter signal in forward model.



Measurements
effected by
Bragg scatter

MBIR Reconstruction with Bragg Rejection

$$(\hat{f}, d) = \arg \min_{f \geq 0, d} \left\{ \underbrace{\frac{1}{2} \sum_{i=1}^M \beta_T \left((g_i - A_{i*} f - d) \sqrt{\Lambda_{ii}} \right)}_{\text{Forward Model With Bragg Rejection}} + \underbrace{\sum_{\{i,j\} \in \chi} w_{ij} \rho(f_i - f_j)}_{\text{Prior Model}} \right\}$$

f : Linear attenuation coefficients to reconstruct (nm^{-1})

$g_i = -\log(\lambda_i)$

$d = -\log(\lambda_D)$

λ_i : Measured BF signal (counts)

λ_D : Unknown Dosage (counts) - can be estimated

$$\beta_T(x) = \begin{cases} x^2 & |x| < T \\ T^2|x| & |x| \geq T \end{cases}$$

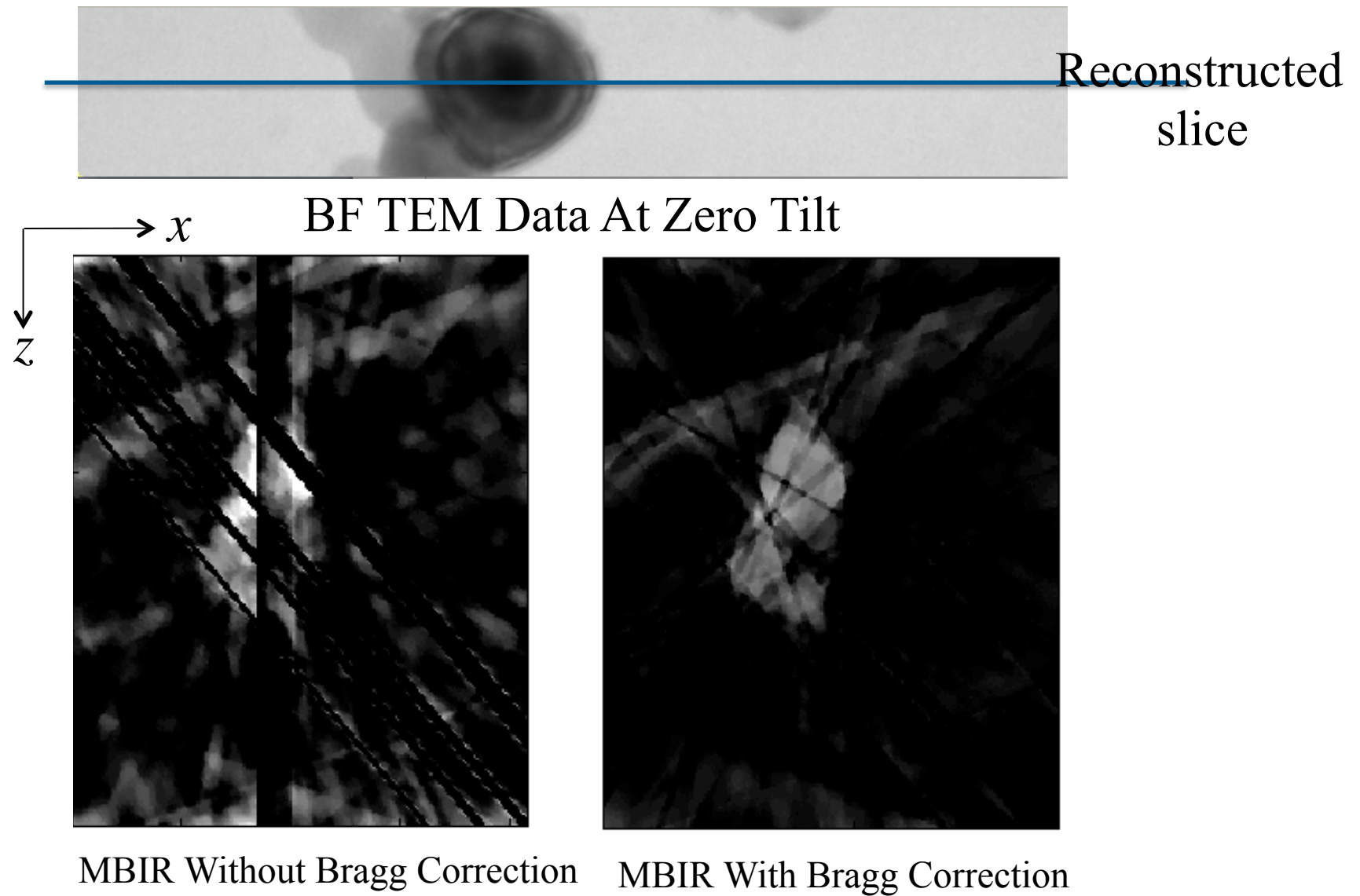
Eliminate the effect of Bragg anomalies

$\Lambda_{ii} : \frac{1}{\text{Noise variance}}$ (scaled) for measurement i

$A_{i*} : i^{\text{th}}$ row of forward projection matrix

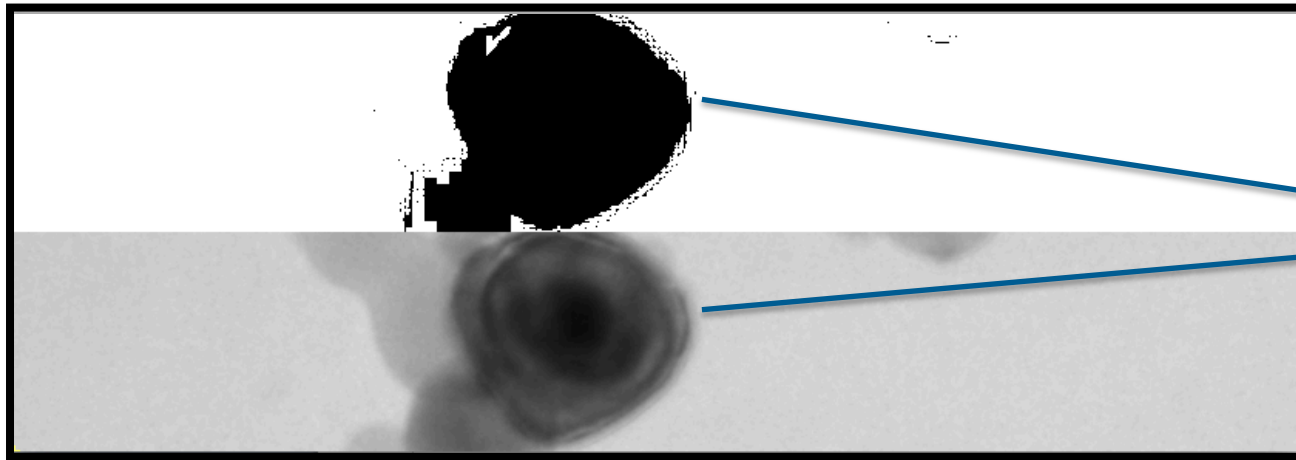
M : Total number of measurements

Reconstruction With Bragg Correction*



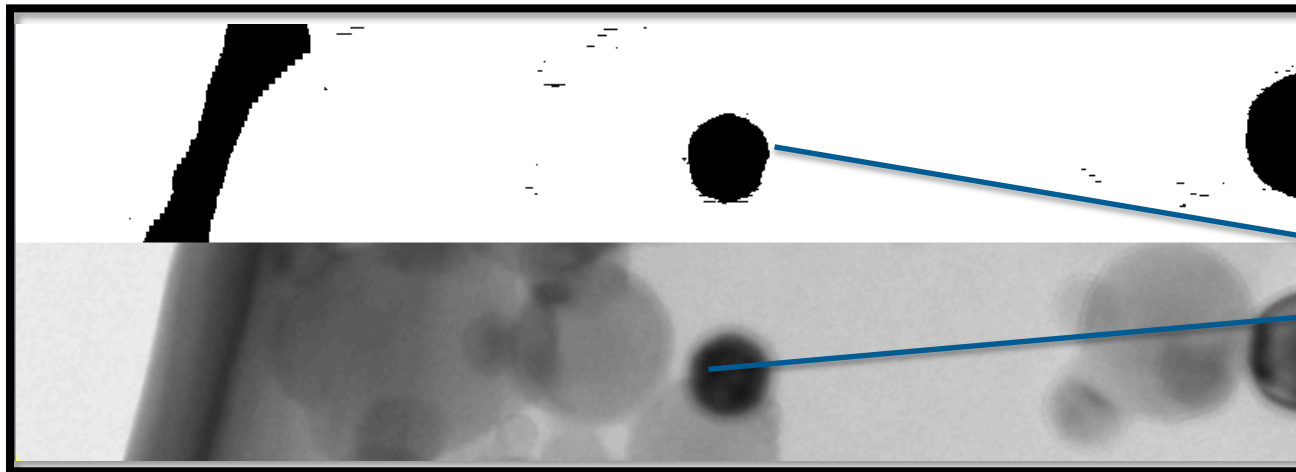
*Lawrence Drummy, AFRL

Bragg Selector and Corresponding Measurement



Bragg
Scatter
detected

Tilt 0

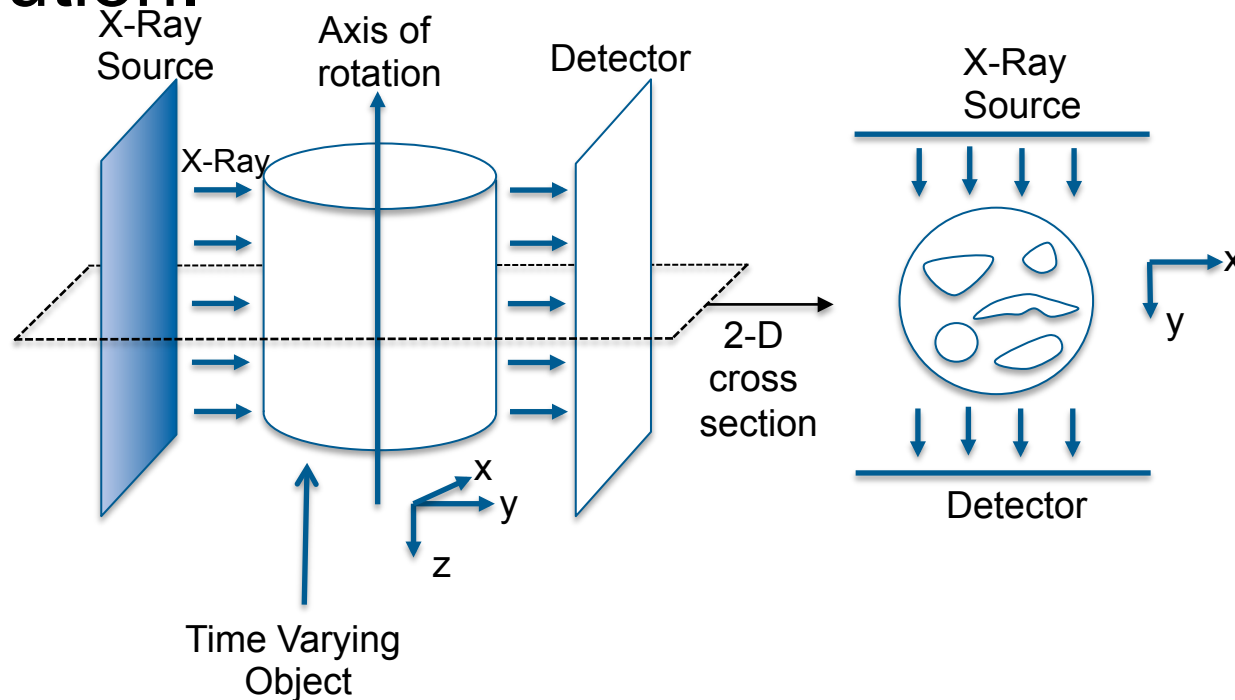


Bragg
Scatter
detected

Tilt +70

4-D CT Imaging of Materials

- Objective: Reconstruct a continuously time varying object at high time and space resolution.



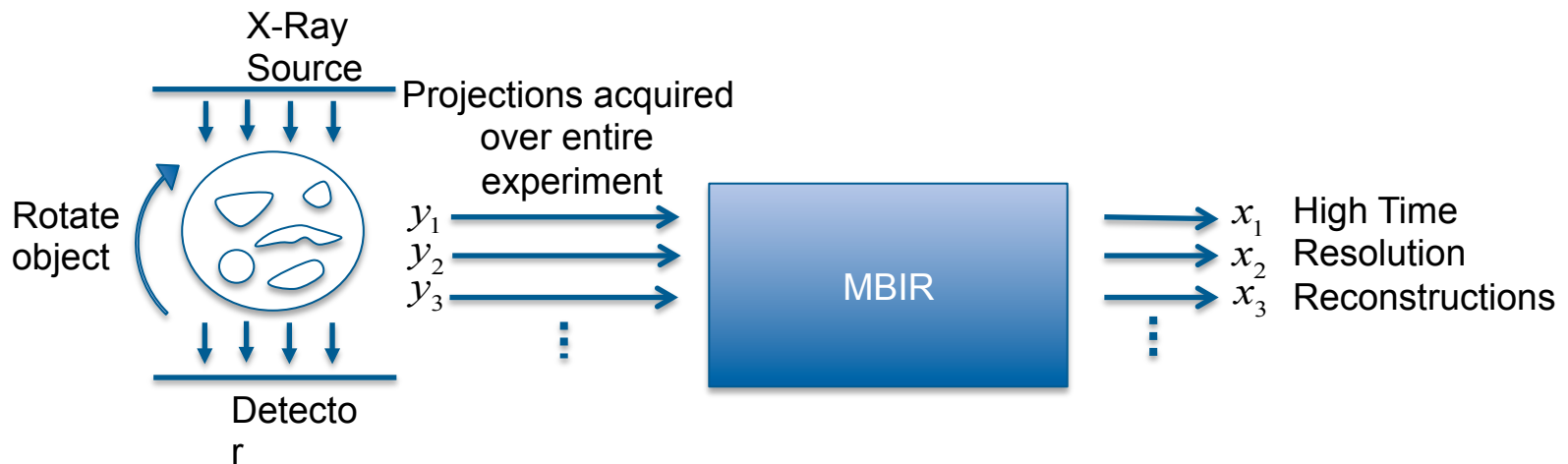
Using MBIR for Time-Space Reconstruction

■ MBIR allows for:

- Reconstruction using any sampling points in time and space
- Projections at any time, angle, location

■ Advantages

- Reconstructs at higher (any) time resolution.
- Accounts for exact time of projection
- Increases envelope of experimental possibilities



MAP Reconstruction Problem for 4-D CT

- Reconstruction is computed by minimizing cost function

$$\hat{x} = \arg \min_x \underbrace{\sum_{k \text{ sample times}} \frac{1}{2} \|y_k - A_k x\|_{\Lambda}^2}_{\text{Forward Model}} + \underbrace{\sum_{i,j \in \Omega_s} w_{ij} \rho_s(x_i - x_j)}_{\text{Prior Model which models spatial correlation}} + \underbrace{\sum_{i,j \in \Omega_t} w_{ij} \rho_t(x_i - x_j)}_{\text{Prior Model which models temporal correlation}}$$

\hat{x} → Reconstructed object

y → Projections

Λ → Diagonal matrix which models the noise

A → Forward projection matrix

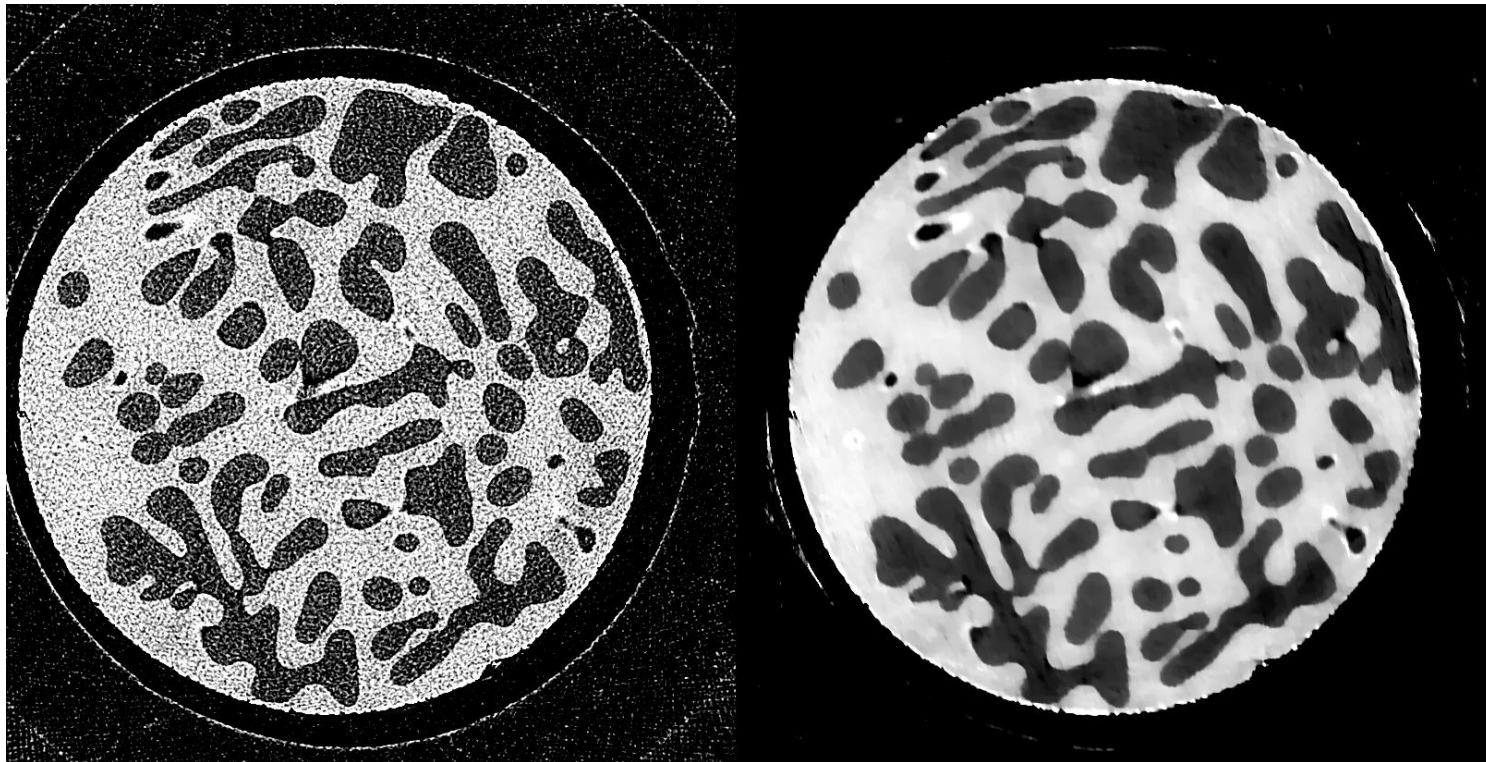
Ω_s → Set of all neighboring voxels in space

Ω_t → Set of all neighboring voxels across time

3-D CT Reconstruction: 2-D space 1-D Time*

Low Time Resolution
FBP reconstruction

MBIR at 4 times the
time



Both reconstructions use 540 projections
acquired over 3 complete rotations of the object

70

**Peter Voorhees, Northwestern University*

Plug & Play Models

Venkat Venkatakrishnan, Purdue

Brendt Wohlberg, LANL

MAP Inversion Framework

$$\hat{x} \leftarrow \arg \min_x \{ l(y; x) + \beta s(x) \}$$

$$l(y; x) = -\log p(y|x) \quad \text{- Forward model}$$

$$s(x) = -\log p(x) \quad \text{- Prior model}$$

- Question: How to mix and match new models?
 - Many new priors: kSVD, bi-lateral filters, non-local means, BM3D, TV, etc.
 - Integrating new priors with sophisticated forward models is difficult!
- Approach
 - Use ADMM to split forward and prior terms.
 - Allows for independent implementation of prior and forward models.
 - Allows for the use of priors without an explicit optimization formulation.

Plug-and-Play Priors Algorithm

Initialize $v = x, u = 0$

Repeat until convergence{

1. $\tilde{x} = \hat{v} - u$

$\hat{x} \leftarrow F(y, \tilde{x}; \lambda)$ //Invert forward model

2. $\tilde{v} = \hat{x} + u$

$\hat{v} \leftarrow H(\tilde{v}; \sigma_n^2)$ //Denoise \tilde{v}



**Plug in any prior -
> only redesign
the denoising
routine !**

3. $u \leftarrow u + \hat{x} - \hat{v}$

}

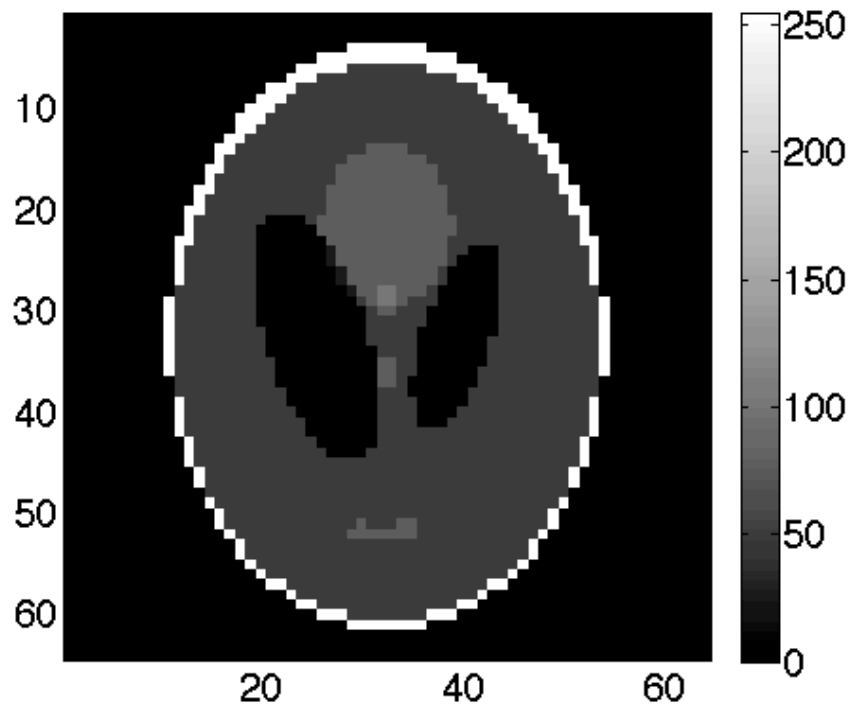
▪Where $F(\cdot)$ and $H(\cdot)$ are independent software modules:

$F(y, \tilde{x}; \lambda) = \arg \min_x \left\{ l(y; x) + \frac{\lambda}{2} \|x - \tilde{x}\|^2 \right\}$ - Model-inversion operator

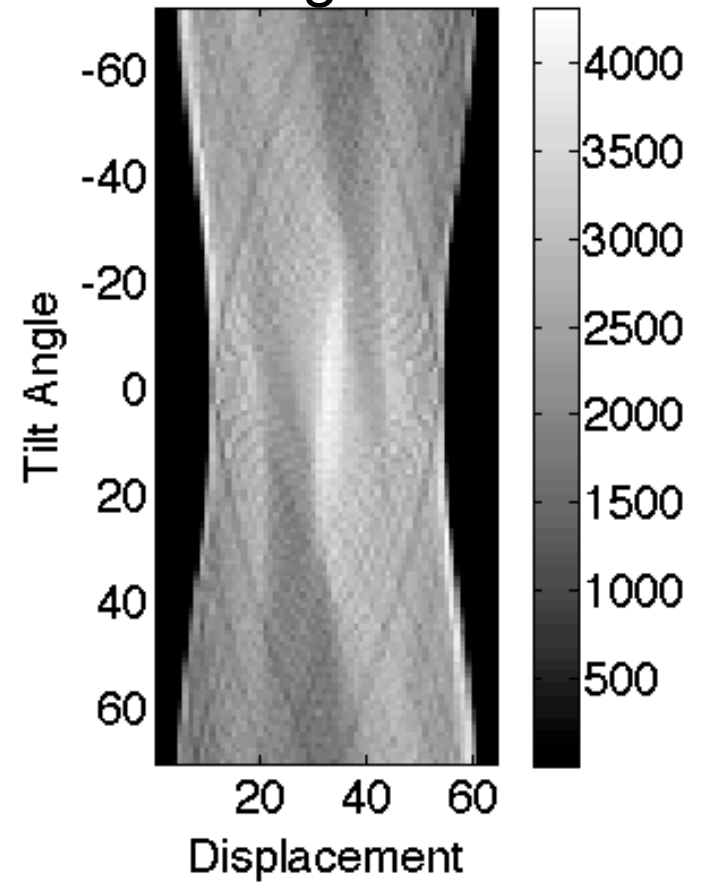
$H(\tilde{x}; \sigma_n^2) = \arg \min_x \left\{ \frac{1}{2\sigma_n^2} \|\tilde{x} - x\|^2 + s(x) \right\}$ - Denoising operator

Data : Phantom and Sinogram

Phantom



Sinogram



Minimum RMSE Reconstructions

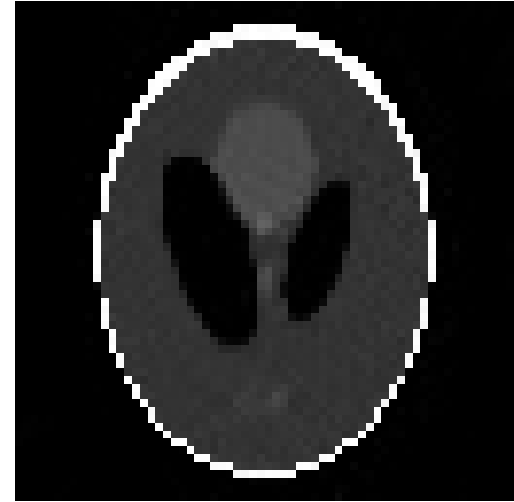
K-SVD



BM3D



PLOW



TV



q-GGMRF



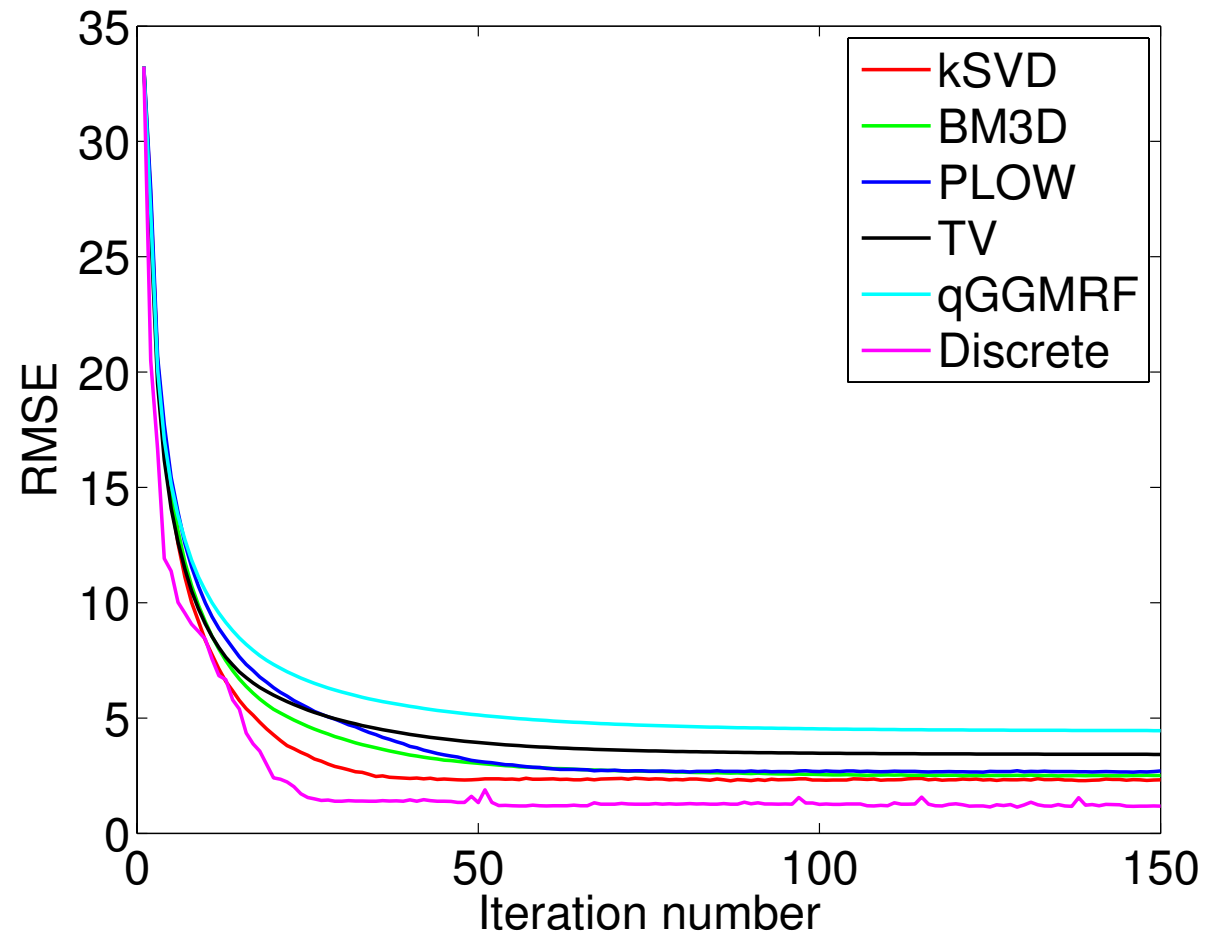
Discrete



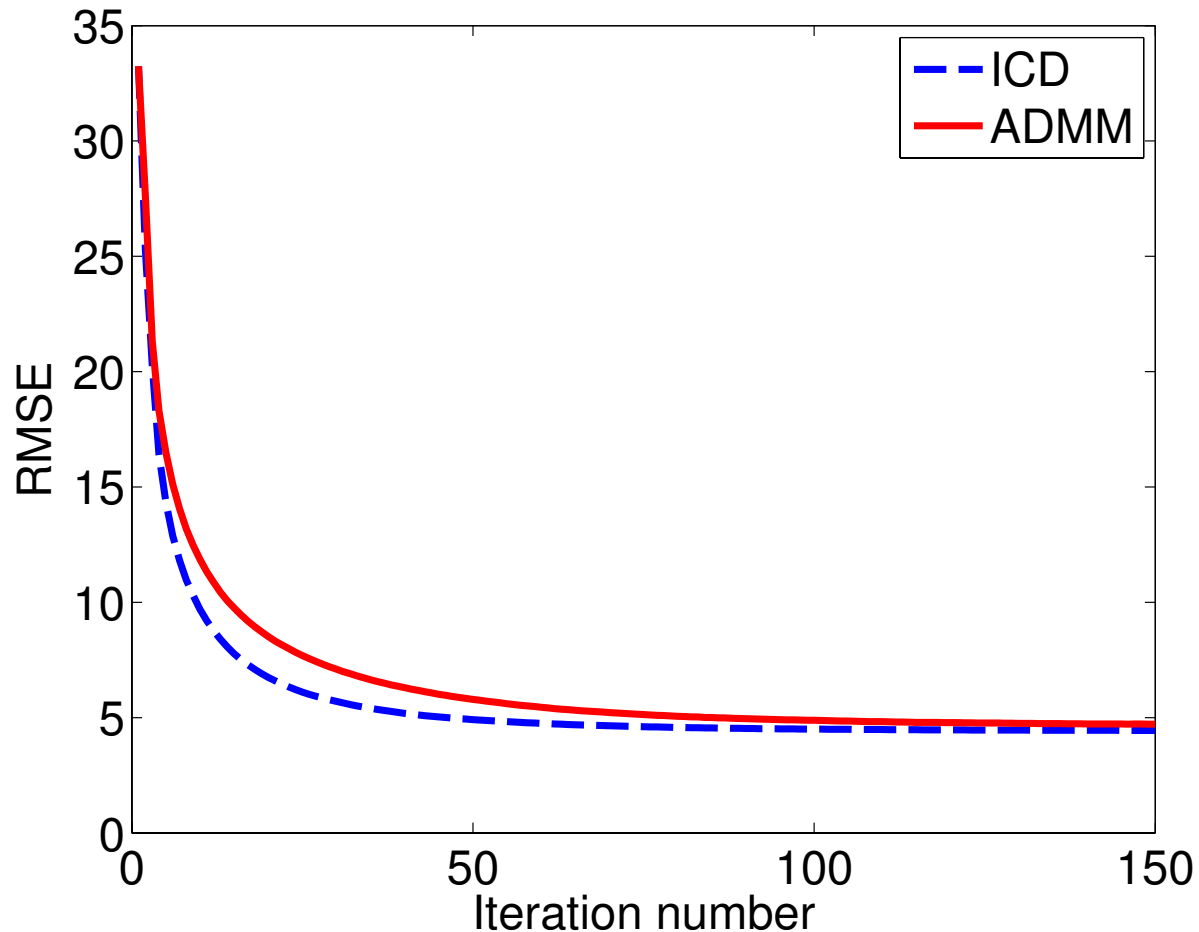
Root Mean Squared Error

Denoising Algorithm/ Prior	RMSE
K-SVD	2.32
BM3D	2.51
PLOW	2.70
TV	3.42
q-GGMRF	4.46
Discrete Reconstruction	1.32

Convergence Plot



Comparison of convergence of ADMM with traditional approach (ICD with q-GMRF [4])



Major directions in Model-based Imaging

- Forward modeling: Account for complex nonlinear parameters and models
- Prior modeling: Account for properties of real images
- Community: Create interdisciplinary teams to solve high impact problems